IEEE Access
Multidisciplinary ⋮ Rapid Review ⋮ Open Access Journal

Received 31 January 2024, accepted 11 March 2024, date of publication 18 March 2024, date of current version 25 March 2024.

Digital Object Identifier 10.1109/ACCESS.2024.3378101

RESEARCH ARTICLE

LED Degradation Monitoring Using a Multi-Channel Spectral Sensor

PAUL MYLAND[1], ALEXANDER HERZOG[1], SEBASTIAN BABILON[2], WILLEM D. VAN DRIEL[3,4], AND TRAN QUOC KHANH[1]

[1]Laboratory of Adaptive Lighting Systems and Visual Processing, Department of Electrical Engineering and Information Technology, Technical University of Darmstadt, 64289 Darmstadt, Germany
[2]Arnold & Richter Cine Technik GmbH & Co. Betriebs KG, 83071 Stephanskirchen, Germany
[3]EEMCS Faculty, Delft University of Technology, 2628 CD Delft, The Netherlands
[4]Signify, 5656 AE Eindhoven, The Netherlands

Corresponding author: Paul Myland (myland@lichttechnik.tu-darmstadt.de)

This work was supported in part by Deutsche Forschungsgemeinschaft (DFG)—German Research Foundation, and in part by the Open Access Publishing Fund of the Technical University of Darmstadt.

ABSTRACT This study explores a novel approach to monitor the spectral emission of LEDs by estimating the spectral power distribution from the spectral sensor responses during an accelerated aging experiment. Two methods for reconstructing the actual LED spectra from sensor responses are presented and tested, one solely requires sensor datasheet information and the other uses a full spectral characterization of the sensor's spectral sensitivities. The reconstruction results show that a spectral sensor can provide accurate spectral estimates even after severe LED degradation. Only for an LED that suffered a phosphor crack, affecting its spatial radiation characteristics, limited ability to estimate the true spectral power distribution without prior assumptions about the spectral changes must be reported. Overall, the use of a spectral sensor, even without detailed characterization of the sensor itself, allows for an accurate monitoring of the true emission of LEDs, with a maximum radiometric error of 0.73 %, a maximum colormetric error of 0.0017 $\Delta u'v'$ and a maximum spectral nRMSE error of 0.0097 compared to a spectroradiometric measurement. This advance holds great promise for improving lighting technology, particularly in applications that require constant radiometric output and stable color.

INDEX TERMS Sensor feedback, spectral sensing, LED degradation, spectral reconstruction, closed loop, spectral power distribution, constant radiometric output, constant light output, stable lighting color, LED maintenance.

I. INTRODUCTION

The research and development of light emitting diodes (LEDs) is closely related to LED lifetime modelling and the associated dependence on operating conditions [1], [2], [3], [4]. Today, there are standardized and established approaches described in the ANSI/IES TM-21 to approximate, model, and extrapolate the radiant flux as a function of operating time, temperature, and current [5]. However, modeling the spectral characteristics is much more complex [6], [7], [8], and significant luminous flux, colorimetric, and spectral errors between state of the art modelling approaches and real degradation data can be observed [9], [10], [11], [12], [13], [14], [15], [16], [17], [18], [19], showing heterogeneity even within sample groups [20]. As a consequence, it is currently unfeasible to use the modeled spectral degradation for proper aging compensation in multi-channel LED systems.

While models could be or already have been developed for the in-situ estimation of LED radiant flux decrease from diode parameters on a chip level [21], [22] or from the electrical and optical small-signal modulation responses [23], there are currently limited possibilities to determine the aging effects that occur in the package from monitoring only the electrical parameters. However, with

The associate editor coordinating the review of this manuscript and approving it for publication was Chao Zuo.

the improvements in crystal quality, device efficiency, and thermal management, the lifetime limiting factors have shifted from the semiconductor chip towards the package elements of the LED system [3]. Defects that may occur on a package level are e.g. delamination, encapsulant yellowing and cracking, tarnishing of the silver reflector, phosphor effects, or cracks [24]. In particular, operation at higher temperatures and low wavelength radiation is known to be associated with decreasing phosphor conversion efficiency and degradation of polymer encapsulants [25].

This paper tackles the issue of LED degradation prediction from a different perspective and addresses the question of whether the actual spectral power distribution (SPD) of a degrading LED can be estimated with sufficient spectral and colorimetric accuracy for lighting applications from spectral sensor responses.

The use of information captured with spectral sensors has already been investigated for various lighting applications. Most of the previous work found in the literature considered RGB-like sensors for modeling and predicting trichromatic responses and/or integral measures of lighting quality: Trinh et al. [26] demonstrated the possibility to estimate the circadian effectiveness of light sources in terms of the circadian stimulus (CS) metric from an RGB color sensor. Agudo et al. [27] developed a portable low-cost color-picking device for non-self-luminous surfaces by combining an RGB color sensor with an integrated high-power white LED. Botero-Valencia et al. [28] proposed a method to estimate the correlated color temperature (CCT) from RGB sensor responses by using linear regression for the transformation from RGB responses to CIE *XYZ* tristimulus values together with McCamy's CCT approximation method [29]. Later, in order to classify artificial light sources into illuminant categories and estimate color temperature and color rendition measures, Botero-Valencia et al. [30] employed a k-nearest neighbor algorithm and category-specific regression models. Breniuc et al. [31] used the raw sensor readouts of an RGBC (RGB + clear silicon channel) sensor to calculate illuminance and CCT values for a tunable-white LED luminaire. Chew et al. [32] and Maiti and Roy [33] both used data from color sensors to model human trichromatic responses directly in the feedback loop of a multi-luminaire lighting system. Ashibe et al. [34] developed a lighting control scheme for a room with 15 RGB luminaires based on color-sensor feedback that allows for the realization of target illuminances and chromaticities at different locations in the room.

As an advancement from simple RGB color sensors, multi-band (i.e., with considerably more than three spectral channels) sensors emerged to fill the gap between (trichromatic) color and spectral information, resolving the spectral energy distribution in greater detail. Botero-Valencia et al. [35] for example developed an alternative to a spectrometer for low-cost spectral light measurements using a multi-layer perceptron (artificial neural network) for the relative SPD reconstruction from spectral sensor responses. Amirazar et al. [36] applied this principle to build a device for monitoring a person's individual lighting exposure from an 18-channel spectral sensor, again relying on an artificial neural network for the SPD reconstruction. Instead of an SPD reconstruction, Botero-Valencia et al. [37] also investigated the feasibility of directly estimating certain color rendition features, such as TM 30-18 R_f and R_g values or the CIE R_a color rendering index, from spectral sensor responses.

None of the published works so far have considered to investigate in detail to which extent a spectral sensor is able to resolve the spectral changes occurring with the degradation of an LED over its lifetime. Such knowledge including an adequate proof-of-concept would open the door to the development of sensor-based multi-channel luminaires that are capable of internally compensating for age-related changes in individual LED channels. As a result, these luminaires could achieve significantly improved color, spectral, and radiant flux consistency over the lifetime of the fixture for factory-calibrated light settings, such as pre-calculated channel mixtures for various CCTs. Here, the current work can be considered to lay the foundation for achieving this goal, firstly, by subjecting four different LEDs to accelerated aging operating conditions while the spectral emission is monitored with a spectroradiometer and a spectral sensor, secondly, by comparing the occurring radiometric, colorimetric, and spectral changes in the LED spectra to the corresponding sensor responses while analyzing potential relationships, and thirdly, by evaluating two different methods for reconstructing the LED spectra from the sensor responses differing in the level of required a priori knowledge about the spectral sensitivities of the sensor. Based on these contributions, the present work demonstrates for the first time the potential in using spectral sensors for monitoring LED degradation.

II. EXPERIMENTAL SETUP AND SAMPLES

A schematic overview of the experimental setup is shown in Figure 1. The LEDs are surface mounted to individual aluminum core printed circuit boards, which are in turn fixed on a copper mounting plate backed by a Peltier element, heat sink and fan. The solder point temperature of the LED boards is sensed with a PT100 resistance temperature sensor and controlled via a THORLABS (Newton, New Jersey, United States) ITC4020 Laser Diode / Temperature Controller. A Keithley (Solon, Ohio, United States) 2651A High Power System SourceMeter is used to drive the LEDs. A switching unit consisting of multiple relays is used to connect the LEDs with the source meter: For optical measurements the switching unit is configured to power one LED at a time, while for the operation condition the LEDs under test are driven in series with constant current. Optical measurements are therefore performed iteratively with only one LED powered in constant current mode by the SourceMeter (switching unit configured to connect the anode and cathode of a single LED to the SourceMeter),

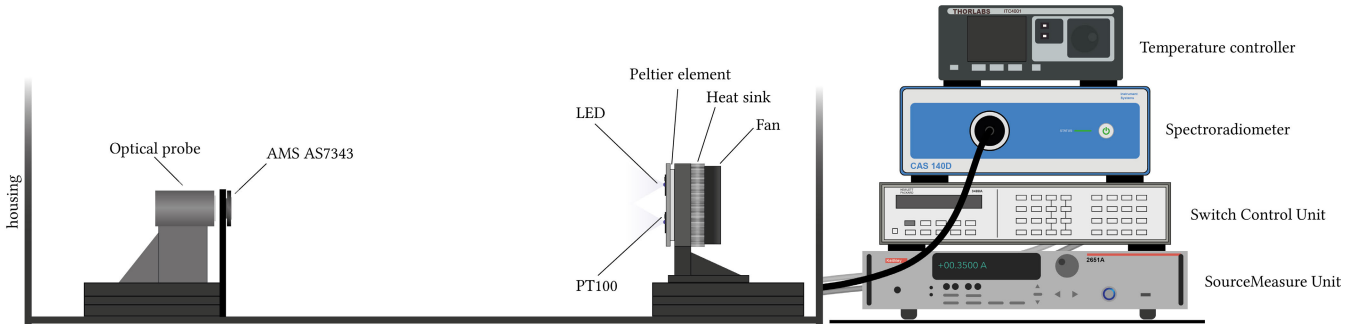

FIGURE 1. Hardware setup with the temperature-stabilized LEDs being oriented towards and aligned with the spectrometer measuring probe and the spectral sensor, all shielded by a black housing. Outside the housing are the temperature controller, the spectrometer, the power source for operating the LEDs and a unit for controlling the circuitry (serial/single) of the LEDs for measurements.

while for accelerated aging with constant stress current, the switching unit is configured to create a series connection of all LEDs under test with the anode of the first LED and the cathode of the last LED connected to the SourceMeter. Spectral measurements are performed with an Instrument Systems (Munich, Germany) CAS 140D spectroradiometer together with an EOP-120 optical probe. The optical probe is facing the LED mounting plate with a distance of 45 cm. The spectral sensor AS7343 from ams-OSRAM AG (Premstaetten, Austria) is mounted with a lateral offset of its optical axis of 5.5 cm to the optical axis of the optical probe.

Since both the sensor and the optical probe approximate a cosine-corrected and diffused angular response (the sensor uses a diffusion foil, the optical probe uses an integrated cosine corrector and diffusion in its glass body), a lateral offset between the sensor and the optical probe could result in a difference in the registered irradiance at the probe and at the sensor position. However, since both SPD estimation methods compute their estimates relative to the initial SPD and the initial sensor response, this difference is already accounted for in the estimation process, making the measurements from the optical probe and the estimates computed from the sensor responses absolutely comparable. This also applies for any color (change) over angle effects of the LEDs. Only if the geometry or directional emission of the LEDs were to change during the experiment would this offset cause errors in the estimation results. The optical components are placed in a matte black housing to shield them from external irradiation.

Four commercially available high power LEDs (one green, one warm white, two neutral white) are subjected to 2000 h of accelerated aging under operating conditions of 1.1 A stress current and a case temperature T_c of 75 °C. Additionally, a fifth LED is acting as a reference, being measured at the same intervals as each of the other LEDs but not being powered the rest of the time and mounted on a separate Peltier element with $T_c = 25$ °C.

Table 1 gives the initial irradiance, illuminance, chromaticity, CCT and Duv (distance of the light source chromaticity to the Plankian locus), while Figure 2 depicts the initial spectral power distributions of the different LEDs with 30 mA

TABLE 1. Initial characteristics (irradiance, illuminance, chromaticity coordinate, and where applicable CCT and D*uv*) of the examined LEDs, measured at 30 mA operating current and 30 °C case temperature T_c. The spectral power distributions are given in Figure 2.

LED	E_r/W	E_v/lx	u'	v'	CCT/K	D*uv*
Green	0.0529	29.9	0.0801	0.5797	-	-
WW	0.0587	18.4	0.2562	0.5148	2902	-0.0061
NW1	0.0574	17.2	0.2210	0.4820	4609	-0.0079
Ref	0.0346	10.9	0.2550	0.5175	2916	-0.0039
NW2	0.0234	7.0	0.2205	0.4758	4824	-0.0106

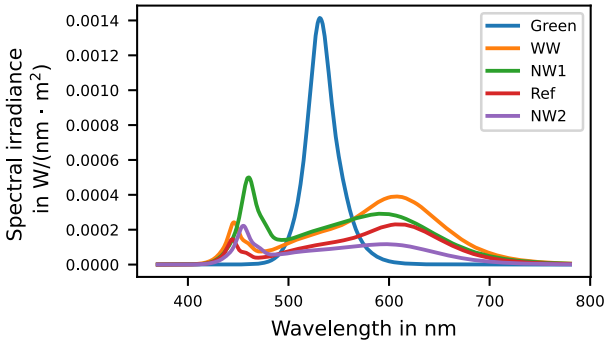

FIGURE 2. Spectral irradiance of the investigated LEDs for the 30 mA, 30 °C measurement condition. The parameters are listed in Table 1.

measurement current at 30 °C measurement temperature. While data was also collected for higher measurement currents, only the 30 mA condition is investigated in this paper, since the effects of defect associated chip-level LED degradation are more pronounced for lower measurement currents [22], [38], [39]. The lowest measurement current is therefore the most challenging condition to test the sensor based spectral monitoring of LED degradation. The measurement cycles are performed in a pulsed manner, where the measurement current is only applied for the duration of the optical measurement defined by the time of collecting the read-outs from both the spectrometer and the spectral sensor. The impact of sensor temperature was disregarded for this experiment, it is not expected to have a significant impact due to relatively stable conditions (mean 30.15 °C and sample

standard deviation 1.64 °C, which were measured using an integrated temperature sensor on the spectral sensor's PCB. Additionally, the sensor was operated with an internal dark current correction utilizing covered photodiodes.

III. SPD ESTIMATION FROM SPECTRAL SENSOR RESPONSES

The electro-optical response of a multi-channel spectral sensor can mathematically be described using Equation (1) [40]. The output value c_k of the kth sensor channel is determined by a non-linear function F, which depends on the sensor's gain factor κ, on the integration time e, and the response signal R. The response signal R is obtained by integrating the product of the spectral irradiance $\phi(\lambda)$ and the channel's spectral sensitivity function $r_k(\lambda)$. Additionally, the term n_k in R represents the contribution of additive noise to the response signal.

$$\begin{aligned} c_k &= F(\kappa, e, R), \\ R &= \int \phi(\lambda) \cdot r_k(\lambda)\, \mathrm{d}\lambda + n_k. \end{aligned} \tag{1}$$

In this work, the AS7343 optical sensor from ams-OSRAM AG (Premstaetten, Austria) with 11 spectral channels in the visible range, an additional clear, and a near-infrared (NIR) channel is used as the monitoring device for the LED degradation. The available evaluation kit of the sensor comes with a diffusion foil attached to the sensor's circuit board. Figure 3 shows the relative spectral sensitivities of the optical sensor system. These sensitivities were determined using an MSH 300 monochromator setup (Quantum Design GmbH, Darmstadt, Germany) with a 300 W xenon arc lamp from 370 nm to 780 nm in steps of $\Delta\lambda$=1 nm, with probe stimuli of approximately 3 nm full-width at half-maximum (FWHM), see e.g. Myland et al. [41] or Trinh et al. [26] for further details.

The sensor features multiple analog gain levels and an adjustable integration time. For the experiment, the gain of 512x was used together with integration times that ensured a sensor saturation of the clear channel of at least 20 %. For the 30 mA measurement current, this implied integration times in the range of 6 s to 25 s depending on the specific LED under test.

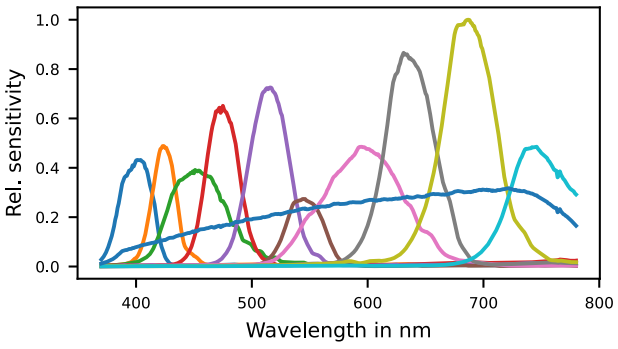

FIGURE 3. Relative sensor sensitivities of the used spectral sensor (AS7343, ams-OSRAM AG). According to the datasheet, the maximum sensitivities of the sensor channels are: 405 nm (actually 401 nm), 425 nm (423 nm), 450 nm (451 nm), 475 nm (475 nm), 515 nm (516 nm), 550 nm (544 nm), 555 nm (560 nm), 600 nm (594 nm), 640 nm (631 nm), 690 nm (687 nm), 745 nm (746 nm). The actual sensitivities were measured on a monochromator with 3 nm full-width at half-maximum (FWHM) and in steps of 1 nm.

Only little preliminary work exist in the literature on reconstructing SPDs from sensor responses and none of them dealt with the reconstruction of spectral, age-related shifts of LEDs. Botero et al. [35] used a multi-layer perceptron (MLP) artificial neural network to reconstruct the SPD of fluorescence, tungsten, and LED spectra mixtures from simulated sensor responses (10 bands distributed in the visible spectrum) to an SPD with a wavelength resolution of 5 nm. The reconstructions are evaluated in terms of SSE R-value, RMSE, NRMSE, CCT error, and multiple color rendition metrics. In summary, NRMSE errors lower than 2 % are reported. Amirazar et al. [36] also made use of an MLP model to reconstruct the SPDs of different light sources from 14 sensor responses to an SPD of 3.5 nm resolution in the wavelength range between 410 nm and 760 nm. NRMSE errors lower than 1 % are reported on simulated sensor data, but errors in a real world validation are considerably higher ranging from 11 up to 40 %. The authors attribute these discrepancies to insufficient training data for the real world application [36].

In a previous work, the authors of the present paper demonstrated the in-field applicability of spectral sensors for spectral reconstruction in real-world lighting scenarios [42], where, on average, spectral deviations of less than 1.6 % in terms of nRMSE, colorimetric error smaller than 0.001 $\Delta u'v'$, and illuminance errors below 2.7 % could be achieved.

Nonetheless, all these preliminary works assume that representative training data for sensor-based SPD estimation are available. In a general illumination scenario, where perfect reconstruction of individual LED spectra is not crucial, but rather the overall satisfactory color and spectral capture of mixtures is of importance, this assumption is justifiable. However, this approach appears inadequate when it comes to accurately reconstructing subtle degradation of individual LEDs without prior knowledge of their aging process for training purposes.

Therefore, a different approach is under evaluation in this work: It basically exploits all the information available in the initial state to enable accurate reconstruction of the specific LED SPDs during operation, but does not include any *a priori* knowledge about possible degradation of the LEDs. For this purpose, two reconstruction variants should be compared, i.e., the estimation via a Wiener filter, which requires knowledge of the spectral sensor sensitivities, and a minimal knowledge approach that works only with key parameters taken from the sensor's datasheet and polynomial-based interpolation between the sensor responses. Both reconstruction variants use the knowledge of the initial SPD of each LED together with the corresponding sensor response to estimate the spectral changes between the initial state SPD and the SPD after a certain number of operating hours under stress

conditions. This drastically reduces the complexity of the otherwise ill-posed reconstruction problem of the spectral irradiance for wavelengths between 370 nm and 780 nm from eleven sensor responses.

A. DIFFERENCE ESTIMATION WITH WIENER FILTER

The Wiener filter [43] approach is an established method for reconstructing spectral reflectance from RGB camera images, when the SPD of the illumination (possibly multiple SPDs time-multiplexed to increase the dimensionality of the captured information) and the camera channel sensitivities are known [44], [45], [46], [47], [48], [49], [50], [51], [52]. Furthermore, the approach has been applied extensively in the field of sensor sensitivity reconstruction from known reflectances and SPDs [53]. In general, the Wiener filter is based on a linear sensor model as described in Equation 2.

$$\mathbf{c} = \mathbf{R}\boldsymbol{\phi} + \mathbf{n}. \tag{2}$$

The sensor response vector $\mathbf{c}$ results from the product of the spectral irradiance $\boldsymbol{\phi} = \phi(\lambda)$ and the sensitivity matrix $\mathbf{R}$ according to the sensor model from equation (1). $\mathbf{n}$ models additive noise on the sensor responses. The estimation from the Wiener filter is then given by

$$\hat{\boldsymbol{\phi}} = \mathbf{W}\mathbf{c}, \tag{3}$$

where the filter matrix $\mathbf{W}$ is computed from the covariance matrix of the SPD to be reconstructed $\mathbf{K}_{\boldsymbol{\phi}\boldsymbol{\phi}} = \langle \boldsymbol{\phi}\boldsymbol{\phi}^{\mathsf{T}} \rangle$, the sensor sensitivity matrix $\mathbf{R}$, and the system noise matrix $\mathbf{K}_{\mathbf{nn}} = \langle \mathbf{n}\mathbf{n}^{\mathsf{T}} \rangle$ according to

$$\mathbf{W} = \mathbf{K}_{\boldsymbol{\phi}\boldsymbol{\phi}}\mathbf{R}^{\mathsf{T}}(\mathbf{R}\mathbf{K}_{\boldsymbol{\phi}\boldsymbol{\phi}}\mathbf{R}^{\mathsf{T}} + \mathbf{K}_{\mathbf{nn}})^{-1}. \tag{4}$$

Since the Wiener Filter is a linear estimator, Equation 3 can also be formulated to estimate the spectral difference $\Delta\hat{\boldsymbol{\phi}}$ from the sensor response difference $\Delta\mathbf{c}$. This uses the knowledge of the initial SPD $\boldsymbol{\phi}_{\text{init}}$ so that only the (compared to the full spectral power distribution) much smaller spectral differences have to be estimated from the sensor response, as shown in Equation 5.

$$\Delta\mathbf{c} = \mathbf{c} - \mathbf{c}_{\text{init}}, \tag{5}$$

$$\Delta\hat{\boldsymbol{\phi}} = \mathbf{W}\Delta\mathbf{c}, \tag{6}$$

$$\hat{\boldsymbol{\phi}} = \boldsymbol{\phi}_{\text{init}} + \Delta\hat{\boldsymbol{\phi}}. \tag{7}$$

Assuming statistical independence of the noise in the channels of the spectral sensor, $\mathbf{K}_{\mathbf{nn}}$ can be constructed as a diagonal matrix with the variance of the sensor responses on the diagonal. The covariance matrix $\mathbf{K}_{\boldsymbol{\phi}\boldsymbol{\phi}}$ is often calculated from a dataset - in case of the reflectance estimation task a dataset of spectral reflectances [45], [49], [52], [54]. The reconstruction quality depends on how well the spectral quantity to be reconstructed can be described by the covariance of the data set, therefore, methods were proposed to weight or select the database entries before reconstruction [55], [56], [57], [58], [59], [60].

Since it is unclear how a data set for a reconstruction of the spectral degradation of an LED should be compiled without already knowing the spectral degradation progression, a more general approach to the construction of the matrix $\mathbf{K}_{\boldsymbol{\phi}\boldsymbol{\phi}}$ is investigated in this paper. This makes use of a matrix with Toeplitz structure according to equation (8) [47], [51], [61], [62].

$$\mathbf{K}_{\boldsymbol{\phi}\boldsymbol{\phi}} = \begin{pmatrix} 1 & \rho & \rho^2 & \cdots & \rho^{n-1} \\ \rho & 1 & \rho & \cdots & \rho^{n-2} \\ \rho^2 & \rho & 1 & & \vdots \\ \vdots & \vdots & & \ddots & \rho \\ \rho^{N-1} & \rho^{N-2} & \cdots & \rho & 1 \end{pmatrix}. \tag{8}$$

The parameter ρ of the Toeplitz matrix can be understood to set the expected correlation between the interpolation points in the spectral distribution. Its optimum value depends on the wavelength resolution and the smoothness of the curves to be reconstructed [53]. In order to incorporate the knowledge about the initial SPD's covariance into the Wiener filter estimation, the matrix $\mathbf{K}_{\boldsymbol{\phi}\boldsymbol{\phi}}$ can be transformed by multiplication of the initial SPD from the left and right as given by Equation (9). This approach equates to weighting the covariance of different wavelengths with their respective power in the initial SPD.

$$\mathbf{K}_{\boldsymbol{\phi}\boldsymbol{\phi},\text{init}} = \boldsymbol{\phi}_{\text{init}}\mathbf{K}_{\boldsymbol{\phi}\boldsymbol{\phi}}\boldsymbol{\phi}_{\text{init}}^{\mathsf{T}} \tag{9}$$

In the literature regarding the reflectance estimation with a Toeplitz-structured estimation matrix, ρ is chosen without further explanation to be 0.97 in two separate studies [47], [51]. For the reconstruction of the spectral sensitivity of a camera, on the other hand, ρ is chosen to be 0.99 [53], which is justified by the smoothness of the expected sensitivity curves of the monochrome sensor and the transmission curves of the filters and by the high wavelength sampling rate of 1 nm steps. In a pre-simulation of the Wiener filter approach for the reconstruction of spectral shifts using spectra composed of up to two Gaussian functions (roughly simulating "white" and monochromatic LEDs), practical values for ρ in the range of 0.79 to 0.91 could be determined (slightly depending on the LED type to be reconstructed). Since LED spectra in general show sharper peaks and, thus, are less smooth than camera spectral sensitivities, such a reduction in optimal ρ values compared to reflectance or sensitivity estimation could be expected. Hence, for this study, $\rho = 0.85$ was used for further computations.

The variances of the sensor response on the diagonal of $\mathbf{K}_{\mathbf{nn}}$ are dominated by photon noise in regular operating conditions of the sensor and, thus, depend on the signal level of each channel [50]. The photon transfer curve (i.e., the variance of the sensor response as a function of the mean sensor response when considering a stable light source) was determined in a separate measurement setup for the given sensor and then used to compute the entries of $\mathbf{K}_{\mathbf{nn}}$ based on the sensor response input to the Wiener filter.

B. DIFFERENCE ESTIMATION WITH SENSOR RESPONSE INTERPOLATION

The aforementioned Wiener filter approach requires knowledge of the spectral sensitivities of the sensor, which can only be accurately determined through elaborated procedures using expensive measurement techniques [41]. Although there are methods in the literature, as mentioned earlier, to estimate the sensitivities of a sensor from more practical setups, it requires to carefully consider how the errors in this sensitivity estimations would affect the reconstruction quality. Therefore, as an alternative method to the Wiener filter, an approach is being investigated that relies solely on basic information about the sensor itself, i.e., the typical peak wavelengths of the individual sensor channels obtained from the manufacturer's datasheet. This is, of course, an imprecise piece of information. However, it is worth noting that the sensor channels already have a certain spectral width that is larger than the specified ranges of variation for the peak wavelengths. Thus, using the information from the datasheet, a rough estimation of the incident energy in specific wavelength ranges can be made from the sensor channels. Between these data points comprising the datasheet peak wavelengths of the channels and the output sensor values, a very rough estimation of the incident power distribution can be obtained by interpolation. However, this would result in an inaccurate estimate of the SPD which is rather inadequate for further use in colorimetric applications. A potential solution is to consider the interpolated sensor responses relative to the initial state of the SPD and the corresponding sensor responses. The spectral changes can be determined as multiplicative factors relative to the initial state by calculating the ratio between the initial interpolated sensor response and any subsequent interpolated sensor response as observed during the aging process. This spectral quotient curve can then be applied to the initial SPD to get an estimate of the SPD at a later time under stress conditions. Even though this approach does not allow for resolving narrowband changes in the power distribution, it still provides a very intuitive method for capturing light output degradation, which is capable of describing at least power redistributions from one broader wavelength range to another, e.g., when examining the excitation peak in relation to the phosphor emission of phosphor-converted LEDs.

Mathematically, the approach can be summarized in a few steps, as given by Algorithm 1. Firstly, interpolation is performed between the eleven sensor responses $\mathbf{c}_\tau$ at a given time τ to match the wavelengths of the spectrometer measurements. Subsequently, the quotient $t_\tau(\lambda)$ is calculated between this interpolation $\tilde{c}_\tau(\lambda)$ and the sensor response interpolation of the initial state $\tilde{c}_0(\lambda)$ for each wavelength. Finally, the initial spectrum $\phi_0(\lambda)$ is multiplied with this spectral ''transmission'' quotient to obtain the estimated spectral power distribution $\hat{\phi}_\tau(\lambda)$.

A plethora of interpolation methods could be employed in step 1 of the algorithm. The classical Sprague interpolation method (according to the CIE recommendation for interpolating spectral data [63]) is not suitable in this case because it assumes that the independent variable is equally spaced. The Sprague interpolation is based on a spline interpolation using 5th-degree polynomials, where the gradients and curvature are constrained to match the neighboring points. Among the various other spline interpolation methods available, the piecewise cubic hermite interpolating polynomial (PCHIP) [64] appears advantageous. It preserves monotonicity, ensuring that no new maxima or minima are created during the interpolation process besides the known data points. Figure 4 shows the described procedure on example data. As can be seen in the caption of Figure 3 the sensor used in this work shows some deviations from the typical channel peak wavelengths given in the datasheet. The effects of the assumed wavelengths and the applied interpolation method are analyzed in the discussion section, showing that the PCHIP interprolation with assumption of the datasheet peak wavelengths is an adequate approach for a minimal knowledge spectral reconstruction. The investigation of this approach aims at determining the quality achievable in the spectral reconstruction of LED degradation without specific sensor characterization.

Algorithm 1 Estimation of Spectral Power Distribution

1: $\tilde{c}_\tau(\lambda) \leftarrow$ Interpolate $\mathbf{c}_\tau$ to match wavelengths of $\phi_0(\lambda)$, with the peak channel sensitivity wavelength λ_k as the assumed wavelength of each channel response c_k
2: $t_\tau(\lambda) \leftarrow \frac{\tilde{c}_\tau(\lambda)}{\tilde{c}_0(\lambda)}$
3: $\hat{\phi}_\tau(\lambda) \leftarrow \phi_0(\lambda) \cdot t_\tau(\lambda)$

IV. RESULTS

First, the aging of the LEDs themselves and the associated sensor responses in the raw state are considered. In particular, the question arises as to whether the sensor is at all capable of detecting changes in spectral emission with its significantly reduced wavelength resolution. Figure 5 shows how the photometric quantities irradiance, illuminance, chromaticity, and RMSE of the normalized spectra (nRMSE) have changed over 2000 h of operation under stress conditions for the individual LEDs. In terms of irradiance and illuminance, the curves are very similar. The green and NW2 LEDs show the strongest degradation of up to 25 % and 10 %, respectively. The other two LEDs under stress conditions, on the other hand, degraded only in the lower single-digit percentage range. Regarding the observed color and spectral deviations, calculated by the distance $\Delta u'v'$ to the start condition in the CIE 1976 UCS and the RMSE between normalized start condition and relative SPDs at later times, there are again similarities in terms of curvature shapes. While the reference LED, as expected, has not undergone any visible changes, the green LED and the warm white LED show slight color and spectral shifts below $\Delta u'v' = 0.0015$ and nRMSE $= 0.006$. The NW1 LED exhibits a steep spectral change within the first 100 h of operating time, which is then continuing with

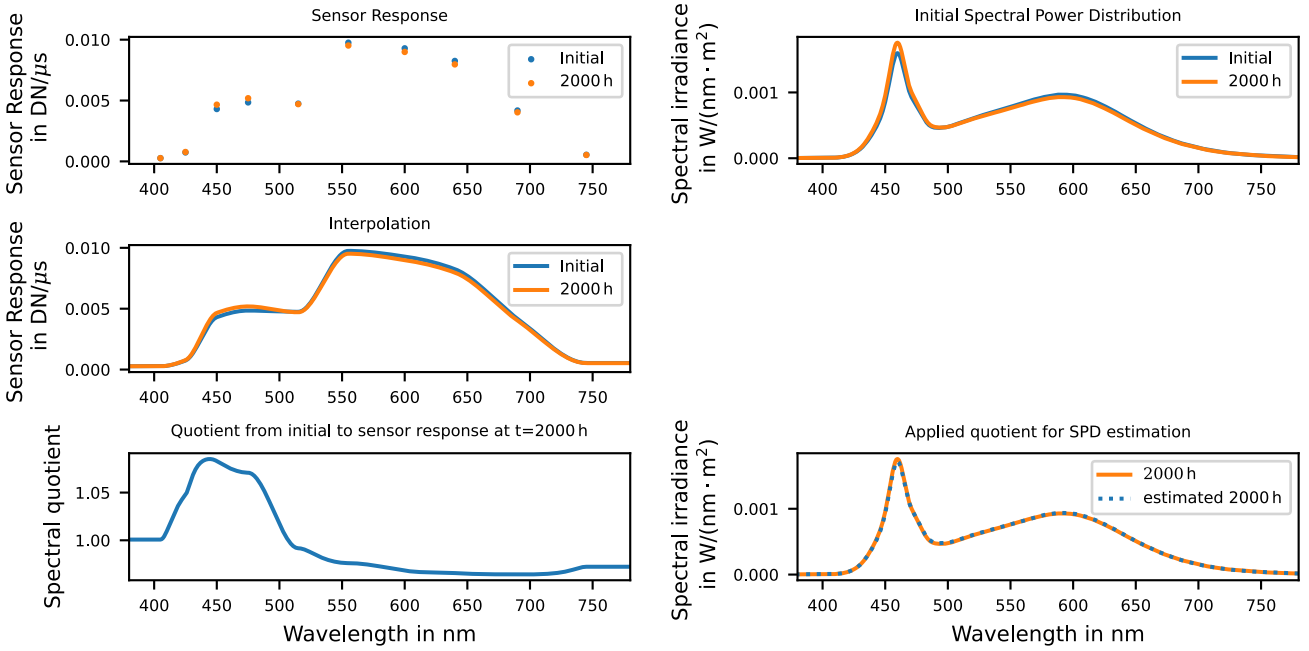

FIGURE 4. Computation steps for the estimation of spectral power distributions from interpolated spectral sensor responses. The interpolation is performed between the sensor responses at a given time. Next, the spectral quotient between this interpolation and the sensor response interpolation of the initial state is computed for each wavelength. Finally, the initial spectrum is multiplied with this spectral quotient to obtain the estimated spectral power distribution.

a slower pace and reaches $\Delta u'v' = 0.0083$ and nRMSE $=$ 0.037 at 2000 h. The NW2 LED shows a steep increase in the first hours, followed by decreasing color and spectral deviations compared to the initial state, while rising steeply again towards the end of the test reaching a high level of $\Delta u'v' = 0.0108$ and nRMSE $= 0.048$ at 2000 h. This can be explained by crack forming in the phosphor layer applied to the LED chip.

The recorded relationship between these spectral changes and the sensor responses of the spectral sensor is visualized in the next three figures. For the sake of clarity, only the LEDs with the greatest aging are depicted: Green, NW1, and NW2. For the green LED, in addition to the differences in spectra and the differences in sensor responses as compared to its initial state, the relative changes given by the actual state divided by the initial state are also shown in Figure 6. As could be seen in Figure 5, aging mainly affects this LED in the form of a decrease in radiant flux. When comparing the differences in spectra to the differences in sensor values, it is clear that this decrease is also detected by the sensor. The relative observation of the spectral changes then shows a minimal shift of the spectral emission towards longer wavelengths, which can also be recognized in the sensor responses. However, it already becomes clear here that the correct interpretation of the sensor data alone (without the knowledge of the causing spectrum) is not trivial. Although the relative changes in the spectra roughly match the relative changes in the sensor responses in terms of their shape, the wavelength range apparently affected by the sensor seems much larger than the SPD changes actually are. This is mainly due to the width of (some) sensor channels (see Figure 3). Nevertheless, the detectable, apparent correlations between measured SPDs and observed sensor responses suggest great potential for reconstructing the spectral degradation dynamics of the green LED.

For the NW1 LED the ratio changes between the light component of the blue excitation chip and the orange component re-emitted by the phosphor over 2000 h of operation. As can be seen from Figure 7, the blue peak of the SPD actually increases with increasing operating time, while the emission of the phosphor in the longer wavelength range decreases. This behavior is also captured by the spectral sensor, which again suggests that the spectral aging process can successfully be reconstructed from the sensor data.

The NW2 LED shows the biggest spectral variations. Essentially, the curves can be divided into two phases: First, the blue part of the spectrum decreases in relation to the phosphor-converted part, until blue light is increasingly emitted directly from the chip of the LED due to crack formation in the phosphor. This is accompanied by a decrease of the phosphor emission, so that after 2000 h more blue and, at the same time, less yellow light than in the initial state make up the total emission. These two aging phases can also be recognized in the differences of the sensor responses with respect to the start condition. However, the crack-related elevation of the blue peak in the second phase of aging as detected by the spectrometer is not reflected in the sensor data. This can be explained by the fact that the strong spectral change of the emission due to the crack in the phosphor may also be accompanied by a change in the spatial radiation

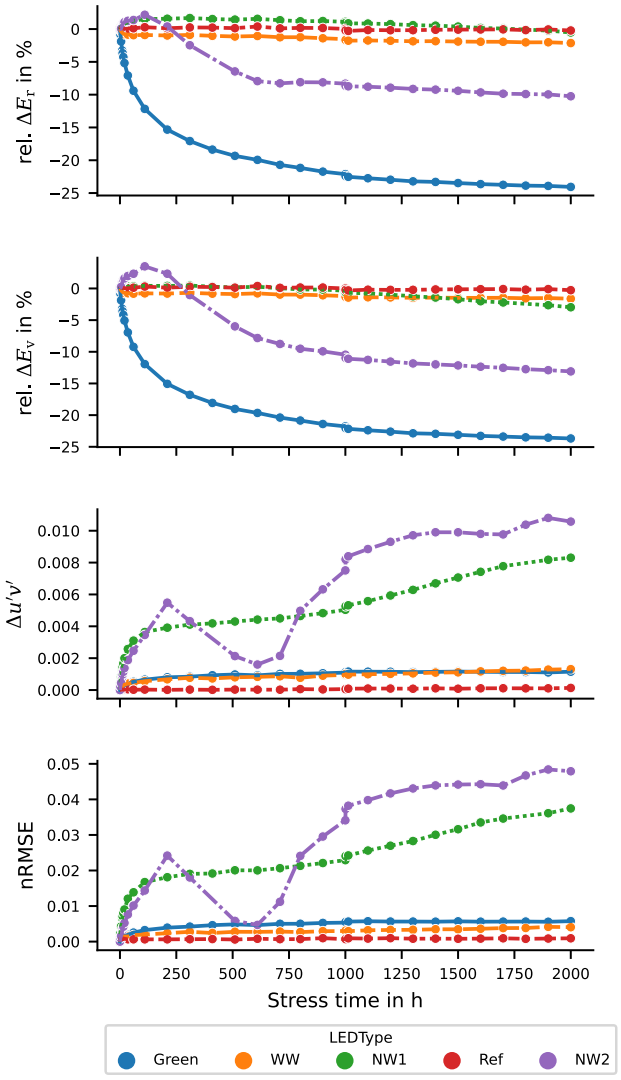

FIGURE 5. Overview over radiometric, photometric, color difference and nRMSE development between the initial measurement at the start of the experiment and later times. The green and NW2 LEDs show the strongest radiometric degradation with up to 25 % and 10 % respectively. The reference LED has not undergone any visible changes, the green LED and the warm white LED show slight, the NW1 LED big color and spectral shifts. The NW2 LED shows a very dynamic curve of color and spectral deviations.

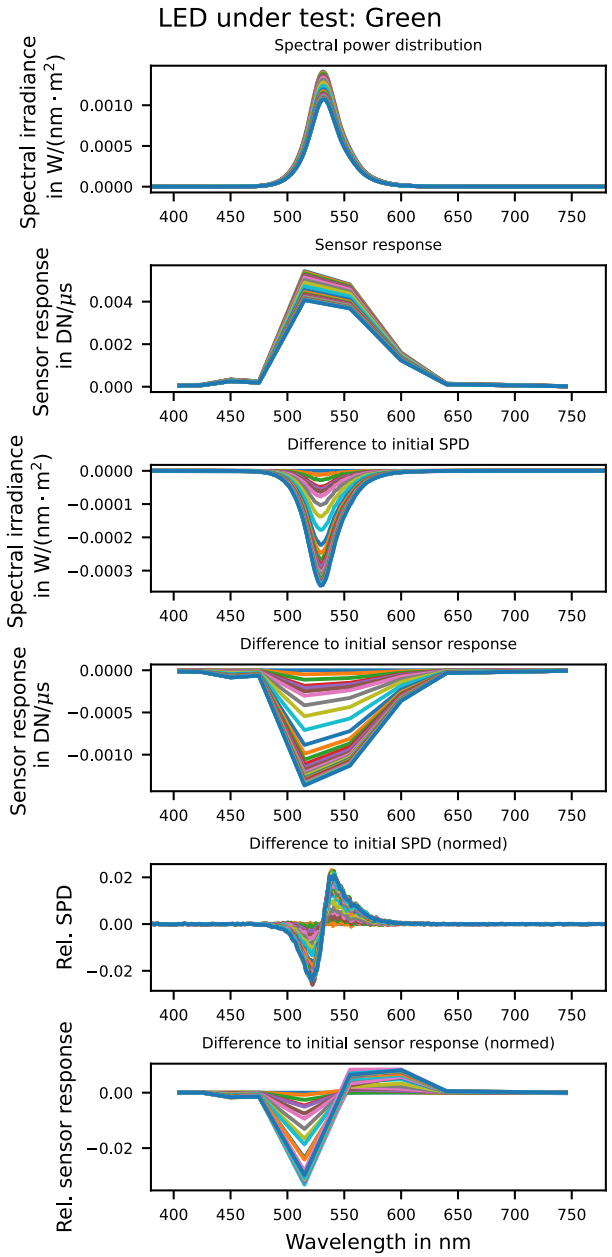

FIGURE 6. Spectral power distributions and corresponding sensor responses for the green LED over the course of the 2000 h stress operation. Also visualized are the differences in spectra and the differences in the sensor responses compared to the initial LED emission at 0 h. A correlation with potential for reconstruction is evident between the sensor responses and the observed spectral behavior.

characteristics. During a test run of the final state of the LED, a clear directional dependence of the light color of the emission could be observed. It is therefore reasonable to assume that the observed discrepancy in the detection of the spectral change between the spectrometer and the sensor is partly due to the spatial distance (5.5 cm, see section II) between the receiver surface of the spectrometer head and the sensor, as the sensor was quite capable of detecting such changes in the blue peak for the NW1 LED. In addition, the changes of the peak at NW2 concern an even narrower wavelength range and are surrounded on both sides by negative spectral differences, which additionally complicates the correct resolving with regard to the already mentioned width of the sensor channels. The NW2 LED therefore is a challenging case for the spectral reconstruction approaches presented in this work, since a very drastic change in the SPD occurred during the experiment. At the same time, most of the spectral degradation is actually captured in the sensor data suggesting that, even in this case, much of the spectral aging process can be successfully reconstructed from the sensor responses.

After presenting the raw data of the aging experiment, the following subsections are dedicated to the analysis of the spectral differences reconstructed from the sensor data with the different methods and their errors.

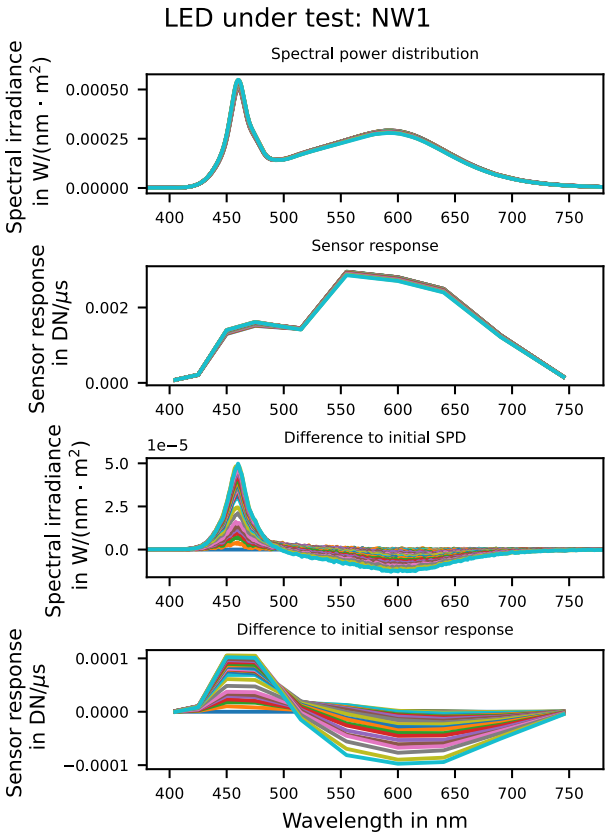

FIGURE 7. Spectral power distributions and corresponding sensor responses for the NW1 LED over the course of the 2000 h stress operation. Also visualized are the differences in spectra and the differences in the sensor responses compared to the initial LED emission at 0 h. A correlation with potential for reconstruction is evident between the sensor responses and the observed spectral behavior.

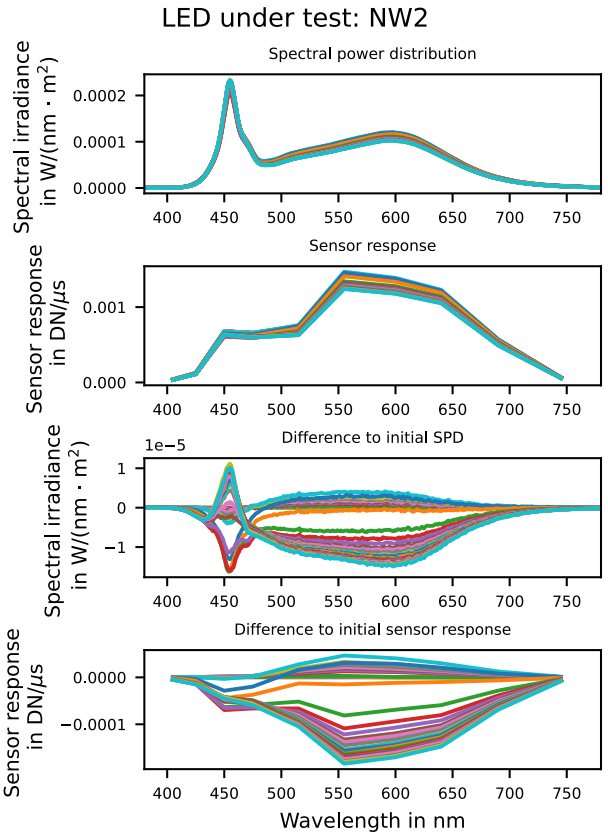

FIGURE 8. Spectral power distributions and corresponding sensor responses for the NW2 LED over the course of the 2000 h stress operation. Also visualized are the differences in spectra and the differences in the sensor responses compared to the initial LED emission at 0 h. Two aging phases can be identified from the differences in the sensor responses and spectra compared to the initial LED state. However, the elevation of the blue peak in the second phase of aging as detected by the spectrometer is not reflected in the sensor data.

A. ESTIMATES OF SPECTRAL DIFFERENCES: GREEN LED

For the green LED, the upper left graph of Figure 9 shows the deviations from the initial spectrum as calculated from the spectrometer measurements. The following graphs in the left column illustrate the reconstruction results using the Wiener filter with a simple Toeplitz matrix $\mathbf{K}_{\phi\phi}$, the Wiener filter with the covariance matrix adjusted via Equation 9, and the PCHIP interpolation approach, which operates without a measurement of the spectral sensitivities of the sensor. It can be seen directly that the generic Wiener filter approach (which knows the spectral sensitivities of the sensor, but apart from the covariance matrix with Toeplitz structure and $\rho = 0.85$ nothing about the difference spectra to be reconstructed) can only estimate the spectral shape of the differences very roughly. Both, the width of the affected area and the position of the actual maximum are reconstructed with considerable errors, as shown in the corresponding residual error graphs depicted in the right column of Figure 9. In contrast, the reconstruction results from both the Wiener filter adjusted to the start spectrum and the PCHIP interpolation are much closer to the ground truth of the true difference spectra. However, neither method can fully track the minimal sideways motion of the emission maximum. This limitation can also be found in the relative ratios of the sensor responses (see Figure 6). The most distinct component of the aging process of the green LED in the form of a decrease in optical power is estimated from the sensor data with little observable error.

The overall performances of the various spectral reconstruction approaches discussed above are visualized in Figure 10 using suitable error metrics. In addition, the error evolution between the initial SPD and the degraded SPDs is given for reference. This basically reflects the current state of most commercial luminaires where no aging compensation from sensor feedback or predetermined by the manufacturer is used. With a similar behavior being observed for radiometric vs. photometric degradation and colorimetric vs. spectral degradation, as shown by Figure 5, the following analysis focuses on irradiance and colorimetric errors only. With regard to the irradiance calculated from the reconstructions, the distance to the initial state (shown in red) increases with time, where after the 2000 h of stress condition the optical power of the green LED actually decreased by approx. 31 %. With the generic Wiener filter,

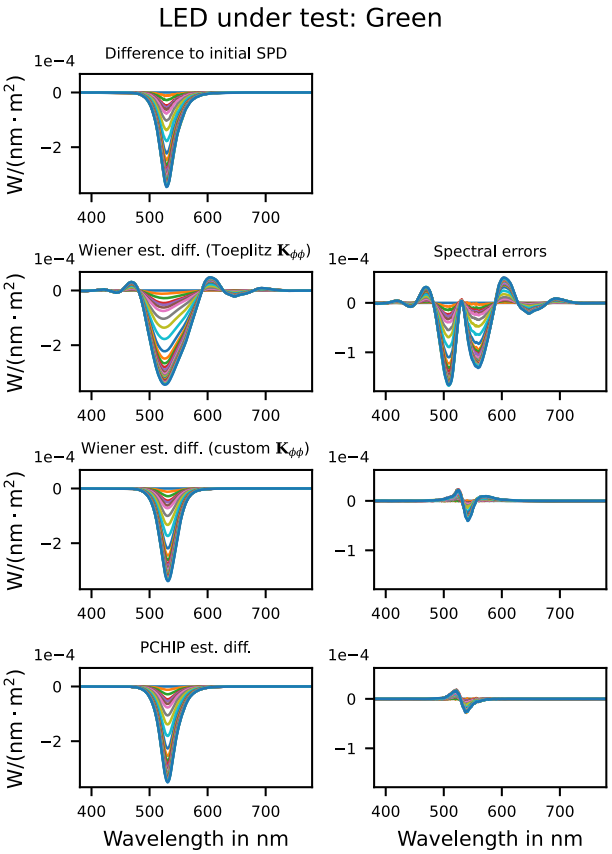

FIGURE 9. Differences to the initial spectrum for the green LED shown together with the spectral reconstruction results for the different reconstruction methods in the left column. The right column shows the spectral errors of the reconstructions compared to the spectrometer measurements at each time. While the generic Wiener filter with the synthetic Toeplitz covariance matrix can only give a rough estimate of the spectral shapes, the spectral errors of the PCHIP approach and the customized Wiener filter are small.

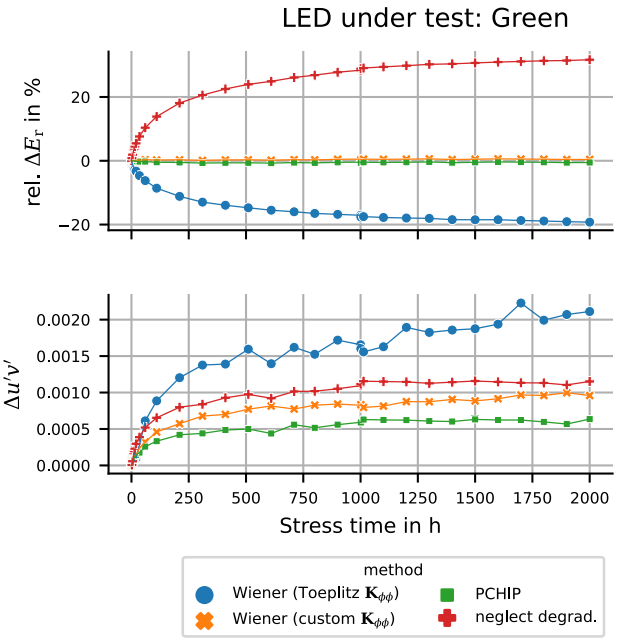

FIGURE 10. Evaluation of the different spectral reconstruction methods compared to neglecting the degradation over the course of the experiment for the green LED. The radiometric error for the adjusted Wiener filter (shown in orange) and the PCHIP interpolation (shown in green) are close to zero at all times. The PCHIP interpolation achieves the best reconstruction result with respect to color deviations.

an underestimation of the optical power of up to 19 % (shown in blue) is observed. In contrast, the irradiance error for the adjusted Wiener filter (shown in orange) and the PCHIP interpolation (shown in green) are much closer to zero. The maximum estimation error in $|\Delta E_r|$ of the adjusted Wiener filter is 0.6 %, while for the PCHIP interpolation a maximum error of 0.73 % is observed.

The green LED undergoes only minimal color changes during this aging experiment so that a maximum error of $0.0012\Delta u'v'$ is made when neglecting the LED degradation. The generic Wiener filter continuously estimates the actual spectrum of the green LED with a larger colorimetric error of $0.0023\Delta u'v'$ at its maximum. The colorimetric error of the adjusted Wiener filter reconstruction, on the other hand, is slightly smaller compared to neglecting the degradation. Here, a maximum of $0.001\Delta u'v'$ is observed. Finally, the PCHIP interpolation achieves the best reconstruction result in terms of residual colorimetric errors showing a maximum of only $0.0006\Delta u'v'$.

For the intuitive analysis of aging processes, a representation of the color coordinates over time as illustrated in Figure 11 is useful [65]. The color coordinates are depicted in CIE 1976 $u'v'$ color space, where the results of the different reconstruction methods, demarcated by color and marker type, are compared to the spectrometer measurements. The time component is visualized by an increasing marker size representing increasing test time. In addition, a scale marker is inserted in the lower left corner with its edge lengths measuring exactly $0.001\Delta u'v'$ to ensure an easy visual assessment of the color distances in the diagram.

As expected from the analysis of the spectral data, the color coordinates of the green LED move roughly on a straight line due to the slight shift of the peak wavelength in the course of the aging experiment. All reconstruction methods correctly estimate the direction of the color changes, but extend towards this direction to different degrees. While the PCHIP approach does not fully track the color shift, the Wiener filters overestimate the shift by indicating higher u' values. Looking at the distance ratios between the starting color coordinates, the final color coordinates, and the estimated color coordinates of all reconstruction methods raises the question of whether an increasingly larger estimation error would be expected with an increasing shift of the LED over time for times beyond 2000 h, where a divergence of the estimates occurs. This question should be investigated as part of future work and can be probed using e.g. a reconstruction experiment looking into current-induced shifts of several nm for a monochromatic LED.

B. ESTIMATES OF SPECTRAL DIFFERENCES: NW1 LED

For the NW1 LED, the spectral reconstruction results and estimation errors are given in Figure 12. The generic Wiener

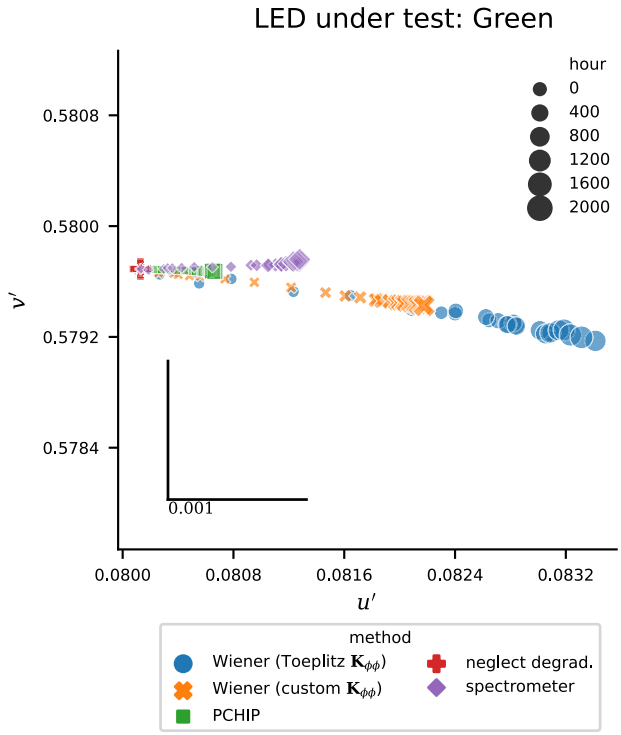

FIGURE 11. The color coordinates of the green LED over the course of the aging experiment. The slight shift of the peak wavelength visible in Figure 6 causes a move of the color coordinates roughly along a straight line towards the direction of orange. All reconstruction methods correctly estimate the direction of the color change. However, the PCHIP approach does not fully track the color shift, whereas the Wiener filters overestimate the shift by indicating higher u' values.

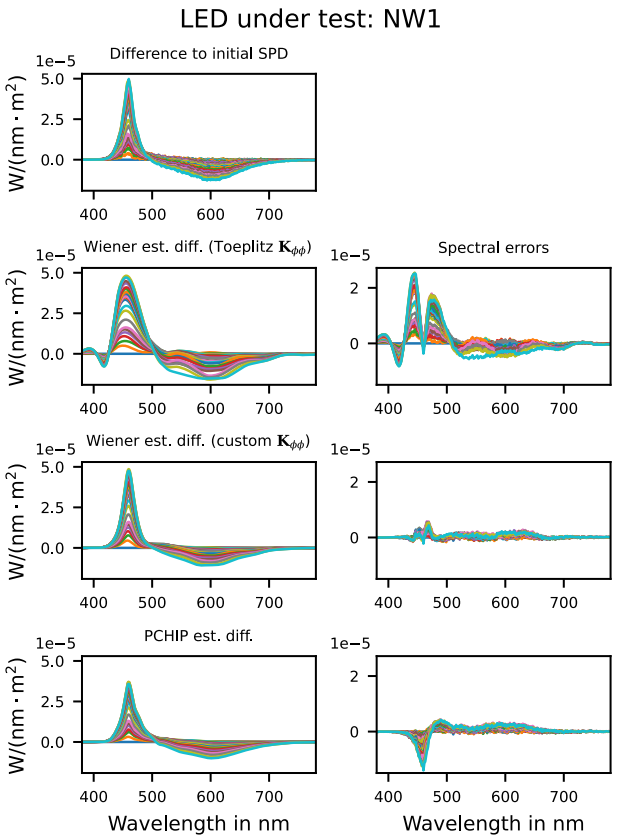

FIGURE 12. Differences to the initial spectrum for the NW1 LED shown together with the spectral reconstruction results for the different reconstruction methods in the left column. The right column shows the spectral errors of the reconstructions compared to the spectrometer measurements at each time. While the generic Wiener filter with the synthetic Toeplitz covariance matrix only achieves a rough estimate of the spectral shapes, the spectral errors of both the PCHIP and the customized Wiener filter approach are much smaller and mainly located around the blue peak, where the latter exhibits the least overall spectral errors.

filter again provides only a very inaccurate estimate of the spectral differences, with significant over- and underestimations especially with regard to the width of the blue peak and its changes. The adjusted Wiener filter shows very small spectral errors in its estimation of the difference spectra, but the largest deviations occur around the maximum of the blue peak. Apart from the blue spectral region, the PCHIP interpolation offers a comparably good reconstruction of the difference spectra, however, the sensor data representing the behavior of the blue peak are interpreted less accurate compared to the adjusted Wiener filter.

The evaluation of the error metrics for the spectral reconstruction of the aging of the NW1 LED is visualized in Figure 13. From the error curves resulting from simply neglecting the degradation it can be seen (similar to Figure 5) that the optical power initially increases slightly and only in the middle progression of the aging experiment a decrease of the optical power occurs.

By neglecting the degradation, maximum relative irradiance errors of 1.65 % are made. Note that the curve shape suggests a further degradation and, thus, increasing errors by neglecting the degradation of the LED for operating times beyond 2000 h. The reconstruction results obtained by using the generic Wiener filter suffers from an overestimation of the optical power in terms of irradiance by a maximum of 1.27 % over large parts of the aging experiment. Both the adjusted Wiener filter and the PCHIP interpolation yield considerably better reconstruction results with a maximum deviation in relative E_r values of 0.55 % for the adjusted Wiener filter and a slightly smaller maximum deviation of 0.4 % for the PCHIP approach. The corresponding relative E_r error curves exhibit a similar behavior and virtually lie on top of each other. Thus, the reconstruction estimates obtained for both the adapted Wiener filter and the PCHIP interpolation approach show much smaller errors than those of neglecting the degradation.

Concerning the colorimetric errors, the latter in comparison to the various sensor-based approaches also yields significantly larger deviations of up to $\Delta u'v' = 0.0083$. Here, even the generic Wiener filter is capable of providing smaller colorimetric errors with a maximum $\Delta u'v' = 0.046$. The error curves for the reconstruction via PCHIP interpolation are even lower, here maximum colorimetric errors of $\Delta u'v' = 0.0017$ are achieved. By far the lowest colorimetric and spectral errors are observed for the adapted Wiener filter

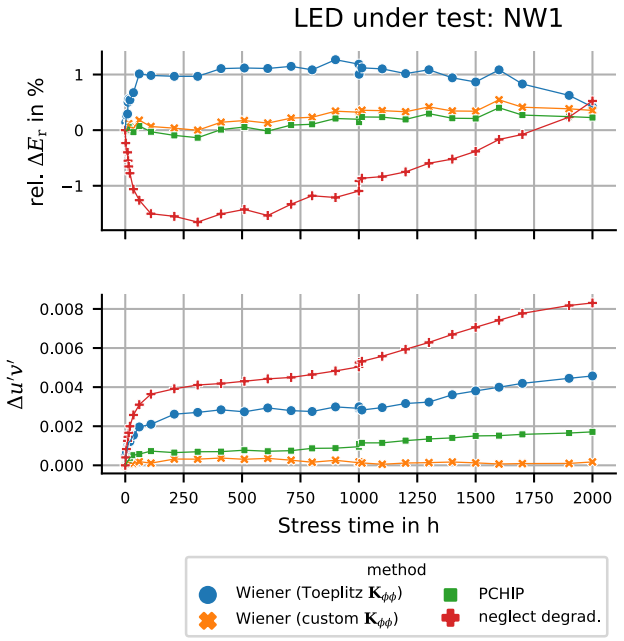

FIGURE 13. Evaluation of the different spectral reconstruction methods compared to neglecting the degradation for the NW1 LED. The irradiance error for the adjusted Wiener filter and the PCHIP interpolation are between 0 and 1 % for all times. The adjusted Wiener filter achieves a spectral reconstruction result with almost no colorimetric errors compared to a spectroradiometer measurement. The observed phenomenon of an increase in irradiance compared to the initial state during the first 1750 h of the experiment is possibly related to the activation of Mg acceptors in the p-region of the diode [39].

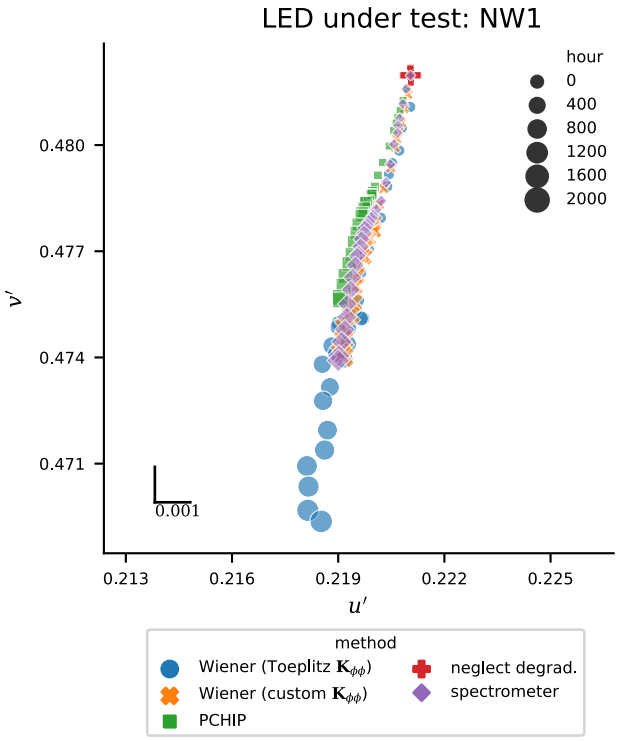

FIGURE 14. The color coordinates of the NW1 LED as a function of time over the course of the aging experiment. The changing ratio between the blue chip emission and the phosphor fluorescence moves the color coordinates towards the direction of blue. All reconstruction methods correctly estimate the direction of the color change. While the PCHIP approach slightly underestimates the color shift, the adjusted Wiener filter tracks it accurately.

approach, where a maximum deviation of only $\Delta u'v' = 0.0004$ can be reported.

Again, the color shifts of the NW1 LED follow an approximately straight line oriented towards the blue part of the color space. As can be seen from Figure 14, all reconstruction methods correctly predict this shift direction. However, the generic Wiener filter overestimates the color coordinates of the LED as being further shifted towards blue than they actually are. The PCHIP reconstruction, on the other hand, again remains a little bit too conservative in its shift estimates, whereas the adjusted Wiener filter follows the course of the spectrometer measurements very closely with an average $\Delta u'v' \ll 0.001$.

C. ESTIMATES OF SPECTRAL DIFFERENCES: NW2 LED

For the NW2 LED, it can be seen from Figure 15 that, as expected, all methods have difficulties in capturing the dynamics of the blue peak in the difference spectra. In addition, the generic Wiener filter also exhibits difficulties in correctly reconstructing the spectral changes of the phosphor-converted light component from the sensor data. Again, the main difference between the adapted Wiener filter and the PCHIP interpolation is in the area of the blue peak. As a result, larger over- and underestimations can be observed for the PCHIP approach when compared to the adjusted Wiener filter.

The erratic nature of the degradation of the NW2 LED is also reflected in the error curves of the different reconstruction methods shown in Figure 16. When considering the E_r errors, neglecting the degradation first leads to an underestimation and later, from about hour 250 onward, to an overestimation of the irradiance with an error of 11.41 %. Again, the generic Wiener filter is unsuitable for determining irradiance with appreciably smaller errors than neglecting the degradation. Here, the reconstruction results of the adjusted Wiener filter and PCHIP interpolation likewise show a transition between the low error start of the experiment and a fairly constant error towards the end of approx. 2 %, where the transition between the two phases can probably be attributed to the cracking of the phosphor.

With regard to the color errors, high variability can be observed. In the initial phase (up to about 250 h), the errors of the reconstruction methods behave in a similar manner as for LED NW1. At this point, the first serious damage to the phosphor appears to set in. Colorwise, the emission of the NW2 LED then consolidates towards the initial state (up to approx. hour 600) and, finally, drifts away with continuously increasing errors. The maximum deviations between the initial and final state amount to $\Delta u'v' = 0.0108$. PCHIP reconstruction and adjusted Wiener filter show a quite similar behavior, where the adjusted Wiener filter reconstructs with smaller errors. In the final state, the color difference between

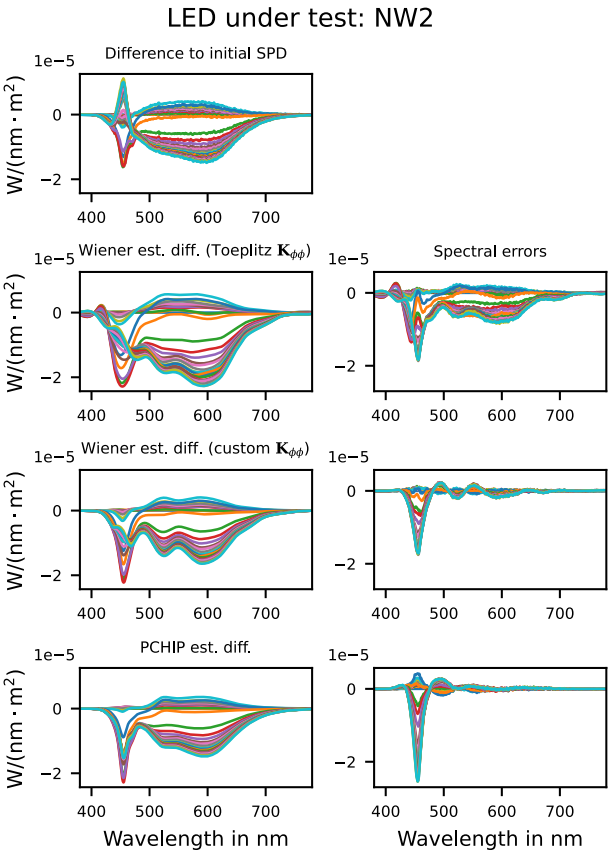

FIGURE 15. Differences to the initial spectrum for the NW2 LED shown together with the spectral reconstruction results for the different reconstruction methods in the left column. The right column shows the spectral errors of the reconstructions compared to the spectrometer measurements at each time. None of the reconstruction methods are capable of delivering an estimate of the later SPDs without notable spectral errors. While the errors of the PCHIP and adjusted Wiener filter approach are mainly around the blue peak of the LED emission due to underestimation, the generic Wiener filter shows spectral errors distributed over the whole wavelength range of emission.

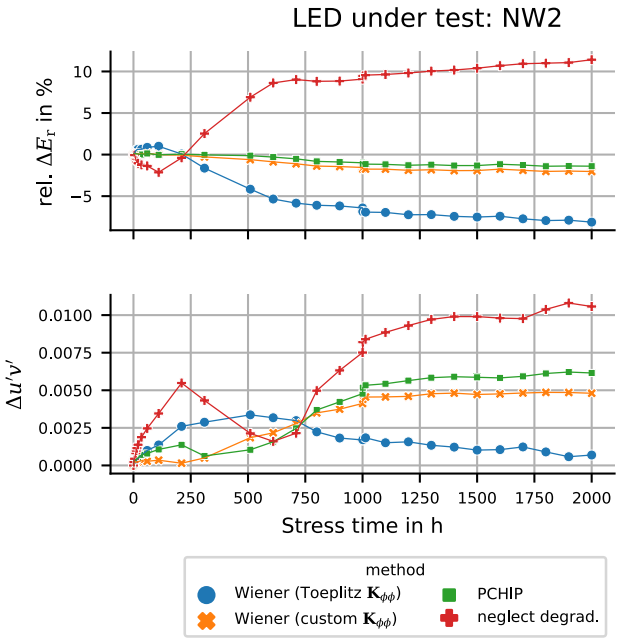

FIGURE 16. Evaluation of the different spectral reconstruction methods compared to neglecting the degradation for the NW2 LED. The radiometric errors of the adjusted Wiener filter and the PCHIP interpolation are between 0 and 2 % for all times. In general, the adjusted Wiener filter and the PCHIP approach achieve a spectral reconstruction result with at least half the colorimetric error compared to neglecting the degradation, but the asymptotic color distance is greater than the human perception threshold of 3 standard deviation of color matching (SDCM) often applied in LED binning (corresponding to a distance of about 0.003 in $u'v'$). The generic Wiener filter appears to outperform the other reconstruction approaches in terms of color estimation error for the later times.

reconstruction and spectrometer measurement is $\Delta u'v' = 0.0062$ and $\Delta u'v' = 0.0049$ for the PCHIP interpolation and the adjusted Wiener filter, respectively.

Even though the generic Wiener filter reconstructs the SPDs of the NW2 LED with the largest errors of all reconstruction methods for the first 250 h, the situation reverses for longer operation and the generic filter achieves very good error metrics at 2000 h. The largest spectral changes were observed with the NW2 LED, which are also reflected in the largest color shifts among the test LEDs as seen from Figure 17. The color coordinates obtained from the spectrometer measurements initially run towards the direction of yellow before taking an almost 180° turn leading to a steady movement towards the direction of blue until the end of the experiment while almost intersecting with the starting color coordinates. This course fits the observed splitting of the phosphor. As already analyzed spectrally and ranked accordingly, the generic Wiener filter delivers the smallest color distances for the later aging phase, while the other reconstruction methods perform better before the observed U-turn in color coordinates.

D. ESTIMATES OF SPECTRAL DIFFERENCES: REFERENCE LED

The reference LED shows no noticeable color shifts ($\Delta u'v' \ll 0.001$) over the 2000 h experiment, as can be observed from Figure 18. The PCHIP results are very narrowly scattered around the spectrometer measurements. The adjusted Wiener filter shows minimal deviations from the LED chromaticity coordinates, while the generic Wiener filter shows $\Delta u'v'$ errors of about 0.001.

E. ESTIMATES OF SPECTRAL DIFFERENCES: WW LED

The WW LED follows a right-hand curve in the $u'v'$ color space, see Figure 19, by first drifting towards blue and then turning towards yellow. All applied methods are capable of reconstructing this course, where, however, an increasing distance of the PCHIP estimates from the true chromaticity coordinates as well as from the chromaticity coordinates of the Wiener filter estimates can be observed.

F. RESULT OVERVIEW

The numerical results for all examined LEDs are presented in Table 2. As expected, only smallest changes, which can be

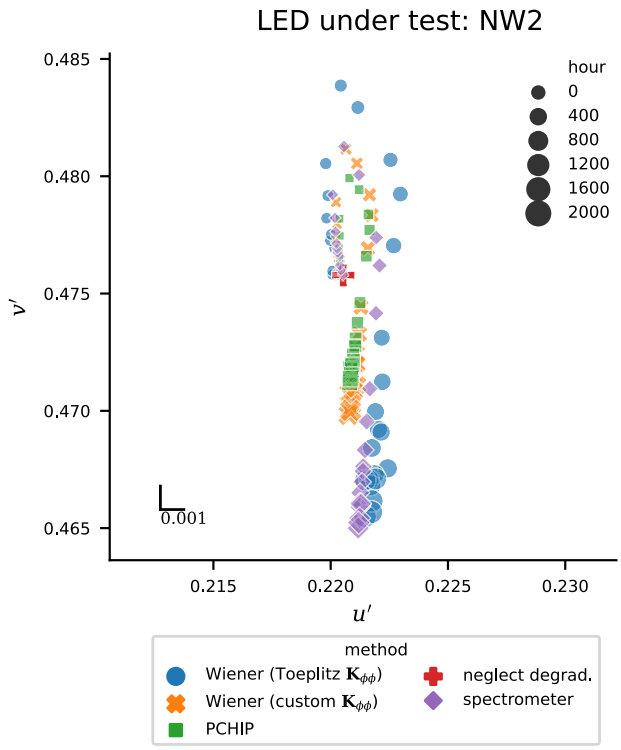

FIGURE 17. The color coordinates of the NW2 LED over the course of the aging experiment. The changing ratio between chip and phosphor as well as a crack in the phosphor cause a dynamic movement of the color coordinates. The color locations initially run towards the direction of yellow, then take a sharp U-turn to move towards the direction of blue. While the other reconstruction methods perform better before this U-turn, the generic Wiener filter delivers the closest color estimates to ground truth for the later aging phase.

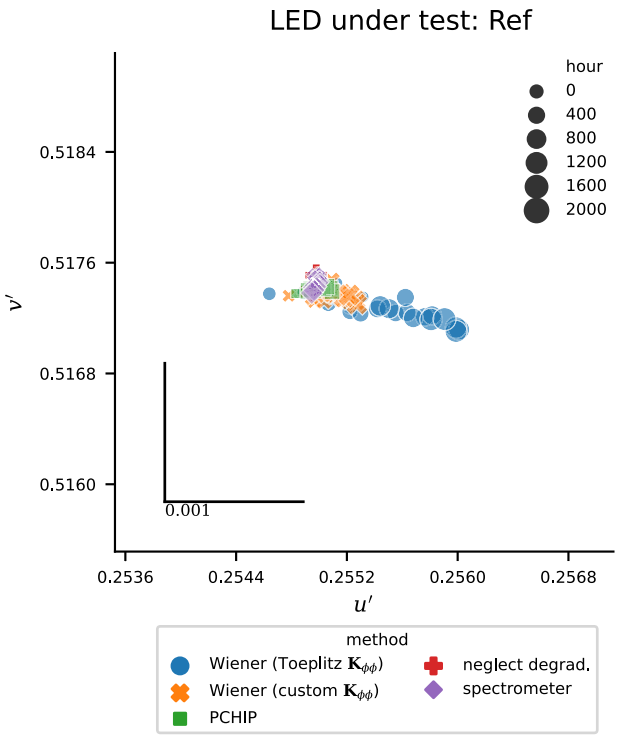

FIGURE 18. The color coordinates of the reference LED over the 2000 h of the experiment. The spectrometer measurements scatter within a very small area (deviations $\ll 0.001$ in u' or v'). The corresponding reconstructions of the PCHIP approach show only a marginally bigger spread. The adjusted Wiener filter shows minimal deviations of the LED chromaticity coordinates, while the generic Wiener filter experiences larger deviations in the same directions as the adjusted one.

interpreted as measurement uncertainties of the spectrometer, occur with the reference LED. Maximal deviations in E_r of 0.38 % and a maximum $\Delta u'v' = 0.000132$ can be reported. The reconstructions of the reference LED sensor data provide almost identical results with the generic Wiener filter showing the largest errors ($\Delta u'v' = 0.0011$). The WW LED also exhibits only small aging effects, where the maximum deviations from the initial state are 2.18 % for E_r and $\Delta u'v' = 0.0013$ in color coordinates. Nonetheless, all reconstruction methods provide considerably more accurate reconstruction estimates than assuming the initial state to be constant (neglecting degradation). Here, a similar pattern as already observed for the other LEDs can be noticed: The generic Wiener filter gives the worst results, the PCHIP interpolation yields the smallest errors with respect to E_r and E_v and the adapted Wiener filter provides the smallest colorimetric and spectral errors.

For lighting applications with a perspective of compensating for the LED aging that occurs for example in a multi-channel LED system, it is rather relevant which errors the reconstruction methods cause or by how much the reconstruction estimates deviate from the ground truth in the worst case. Therefore, for the evaluation of the reconstruction results, the maximum errors are discussed. Comparing with the results obtained for the other LEDs from this experiment, the very good color and spectral performance of the generic Wiener filter for the NW2 LED seems to be a coincidence here, which will be reasoned in the discussion section.

V. DISCUSSION

The reconstruction results from the previous section provide room for discussion. For the results of the green LED the generic Wiener filter is limited in its ability to estimate the spectral degradation because a covariance matrix with Toeplitz structure and constant correlation parameter ρ over the whole wavelength range is assumed. This is a severe disadvantage, because the actual LED emission is situated in a very narrow wavelength range, and the spectral changes resulting from the degradation are also very narrow. On the other hand, there is a wide sensor channel (peak approx. 555 nm, FWHM approximately 100 nm) and neighboring channels whose sensitivities only intersect at the edges with the emission of the green LED. The generic filter is therefore set up (from the Toeplitz-covariance matrix) in such a way that the changes in the sensor responses from the initial measurement, are estimated to happen over the entire range of sensitivities of the sensor channels registering the LED emission, which leads to the overshoots and undershoots in the estimated difference spectra in Figure 9 for the generic

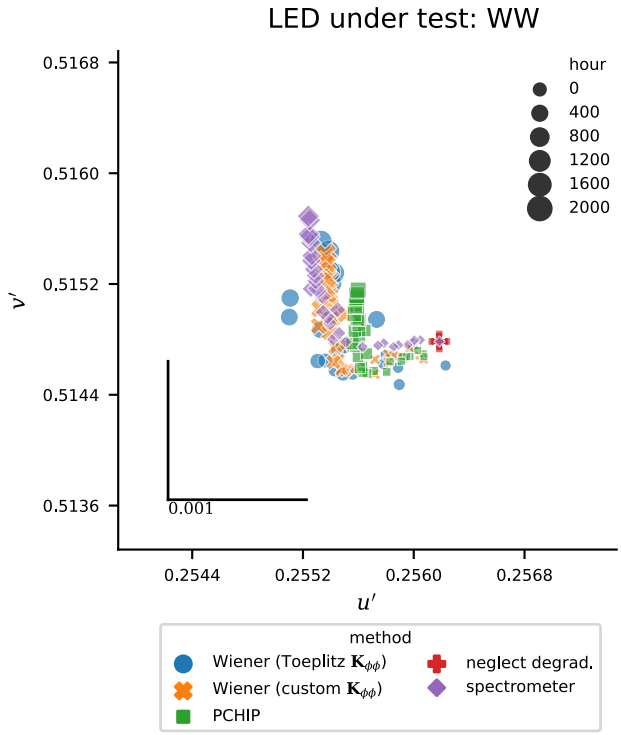

FIGURE 19. The color coordinates of the WW LED over the course of the aging experiment. The color coordinates first move towards blue and then turn towards yellow. All applied methods are capable of reconstructing this course, but the PCHIP results show an increasing distance to the spectrometer measurement after the turn.

TABLE 2. Maximum errors of irradiance, illuminance, color and spectral distribution between a sensor-based reconstruction and a spectrometer measurement, broken down by method and LED type.

LED	method	$\widehat{\lvert\Delta E_\mathrm{r}\rvert}$/%	$\widehat{\lvert\Delta E_\mathrm{v}\rvert}$/%	$\widehat{\Delta u'v'} \cdot 10^{-3}$	$\widehat{\mathrm{nRMSE}}$
Green	PCHIP	0.728	0.983	0.636	0.005
Green	Wiener (Toepl.)	19.235	17.432	2.228	0.049
Green	Wiener (custom)	0.601	0.189	0.997	0.007
Green	negl. degr.	31.688	31.036	1.158	0.006
NW1	PCHIP	0.402	0.854	1.711	0.010
NW1	Wiener (Toepl.)	1.267	1.230	4.571	0.013
NW1	Wiener (custom)	0.545	0.555	0.372	0.003
NW1	negl. degr.	1.653	3.058	8.307	0.037
NW2	PCHIP	1.404	0.451	6.213	0.031
NW2	Wiener (Toepl.)	8.125	7.977	3.365	0.012
NW2	Wiener (custom)	2.034	0.714	4.859	0.018
NW2	negl. degr.	11.413	15.069	10.805	0.048
Ref	PCHIP	0.350	0.385	0.183	0.001
Ref	Wiener (Toepl.)	0.321	0.308	1.085	0.008
Ref	Wiener (custom)	0.341	0.331	0.327	0.003
Ref	negl. degr.	0.384	0.384	0.132	0.001
WW	PCHIP	0.484	0.272	0.644	0.003
WW	Wiener (Toepl.)	0.455	0.388	0.488	0.004
WW	Wiener (custom)	0.597	0.497	0.329	0.002
WW	negl. degr.	2.177	1.648	1.310	0.004

Wiener filter. The generic filter simply lacks the information to provide a better estimate: The spectral changes to be reconstructed are too narrow compared to the width and number of sensor channels observing these changes, and the unadjusted (generic) covariance matrix does not help to narrow down where in the spectral range the spectral changes are located. The adjusted (covariance) Wiener filter in comparison is mathematically constructed to estimate the spectral changes to occur in regions where the initial SPD had the most power, which in the case of the green LED reduces the estimation errors for the Wiener filter greatly. The even still slightly better performance of the PCHIP approach for the green LED can be reasoned by the fact that almost no spectral (sideways) shifts occur, and that the simple interpolation of sensor responses introduces smaller errors than an ill posed (eleven sensor channels to 401 wavelengths) Wiener estimation for this case. Nevertheless, the latter two reconstruction methods show a very good spectral traceability of the aging of the green LED via the output values of the spectral sensor.

In the case of the NW1 LED, the adapted Wiener filter approach can show its benefits from knowledge of the spectral sensitivity curves of the sensor and, thus, in addition to low errors with regard to E_r and E_v, also achieves an excellent spectral estimation of the actual SPD of the LED after severe aging. The results of the PCHIP interpolation, on the other hand, are also still in a very good range, i.e., $\ll 2$ SDCM, which would be classified as a barely perceptible difference in the context of LED binning.

Unfortunately, concerning the results of the NW2 LED, it is not possible to determine from the data of the experiment by how much the phosphor crack affects the spatial radiation characteristics of the LED. Thus, in addition to the error stemming from the applied reconstruction method itself, an unclear impact of potentially different irradiances on the spectrometer head and the spectral sensor is to be expected. The observation that the reported errors for the illuminance estimates are small and almost without any visible impact from the phases of the phosphor crack can be explained by the fact that the reconstruction errors in Figure 15 are found to especially occur in the blue region, which basically has not much relevance for the $V(\lambda)$ weighted illuminance.

Regarding the results of the NW2 LED, the surprisingly good performance of the generic Wiener filter approach in terms of color and spectral errors demands for further discussion: The good performance of the generic Wiener filter for the NW2 LED appears to be a coincidence, because for all other LEDs this method offers by far the worst estimation results. Even for the NW2 LED, looking at the residual spectral errors (Figure 15), it is not apparent that the generic Wiener filter provides a better spectral reconstruction (compared to the other methods). Only when the colorimetric integrals are evaluated in terms of $\Delta u'v'$ the generic wiener filter pulls clearly ahead. This can be explained from the trichromaticity of human color perception, where color is assumed to be describable by a relation between radiation in the short (around 450 nm), medium (around 555 nm) and long (around 600 nm) regions in the visible spectrum. Comparing

the different spectral residual errors between the estimation methods in Figure 15 it becomes apparent, that the error of the generic Wiener filter is distributed over the whole visible region, while the errors of the adjusted Wiener filter and PCHIP approach are concentrated in a sharp peak around 460 nm. The generic Wiener filter clearly overestimates the changes in the yellow-orange light component as the estimated spectral differences in Figure 15 are clearly more negative than calculated from the measured ground truth or from the other reconstruction methods. These different error distributions lead to a smaller colorimetric error for the generic Wiener filter compared to the other methods, because the ratio between the three tristimulus values is less effected from the more evenly distributed spectral error of the generic Wiener filter. Comparing this performance with the performance on the other LEDs it is clear that the generic Wiener filter is generally more imprecise in it's spectral reconstruction than the other methods (broader error distributions). Only for the NW2 LED this coincidentally results in a smaller colorimetric error, that is accompanied by a large radiometric error. In principle, however, it is of course possible that the generic approach provides better results for LED changes that cannot be described with the covariance matrix adjusted to the initial state. Further investigations with other LEDs and scenarios are required in a follow-up to this work to reveal whether the more unspecific reconstruction of the unadjusted Wiener filter can actually be an advantage in certain cases.

The comparison of the results from both Wiener filter variants frequently shows similar directions in terms of deviations, possibly caused by inaccuracies in the spectral characterization which are manifested here. This represents a reopening of an old topic, as the spectral characterization of cameras has been the subject of extensive research in numerous publications in the past [66], [67], [68], [69]. Simultaneously, spectral sensors for spectral reconstruction significantly raise the bar for required characterization accuracy. When considering camera sensitivities, there can be a general assumption of a certain smoothness in the spectral sensitivities, as the sensitivities of different channels are realized through pigments or dyes, rather than nano-optical interference filters, as it is the case for most spectral sensors. Moreover, the spectral sensor sensitivities exhibit much steeper slopes compared to most RGB cameras. At this point, it is very convenient for the practical application that the PCHIP approach based only on the datasheet properties of the sensor was already able to reconstruct the degraded spectral emission of all LEDs in this experiment very well.

To analyze the impact of deviations in real channel peak wavelengths from the datasheet on the accuracy of the minimal knowledge approach (PCHIP) the assumed peak wavelengths are varied in 5 nm steps within ±10 nm of the typical value for all sensor channels in the NW1 LED's radiation range, resulting in 390625 combinations of peak wavelengths. The resulting errors of different assumptions of peak sensitivity wavelengths are given in table Table 3. Assuming different peak locations can lead to smaller or larger errors in individual metrics compared to using measured peak wavelengths or typical values from the datasheet, while no peak wavelength assumption minimizes all evaluation metrics at the same time. The datasheet values provide a performance close to the median of all possible combinations; for the actual sensor used in this experiment, there is no observable benefit in using the laboriously measured true peak locations. The PCHIP approach is therefore limited by the width and number of the sensor channels, the (in)correct assumption of the datasheet channel peak sensitivity wavelengths only has a minor influence on the performance of the PCHIP approach for the given sensor. The assumption of the typical peak sensitivity wavelengths (datasheet) offer close to median performance of all possible assumptions.

TABLE 3. Monitoring result variations caused by assumption of different channel peak wavelengths for the PCHIP approach in reconstructing the NW1 LED after 2000 h stress operation. Given are the minimal, median and maximum resulting error in comparison to the results of using the datasheet peak locations and the measured peak locations of the actual sensor (Figure 3).

	$\Delta E_r/\%$	$\Delta E_v/\%$	$\Delta u'v' \cdot 10^{-3}$	nRMSE
Minimum	-0.27	0.34	0.0012	0.0057
Median	0.17	0.67	0.0017	0.0088
Maximum	0.61	1.06	0.0022	0.0107
True peaks	0.19	0.68	0.0016	0.0086
Datasheet peaks	0.17	0.66	0.0017	0.0087

The impact of the interpolation method can be discussed on the basis of Table 4, where the mean and maximum value for the evaluation metrics are shown for minimal knowledge spectral reconstructions from senor data of all LEDs under stress conditions after 2000 h using different algorithms for the interpolation step. A simple form of interpolation can be achieved through polynomial regression from the sensor responses as dependent variables and the assumed peak channel sensitivities as independents. The evaluation metrics for using such a polynomial interpolation of order 1, 3, 7 and 11 are given in the table.

As introduced in the methods section of this work, the CIE recommendation for interpolating spectral data [63]) is based on spline interpolation, so for comparison of interpolation methods for sensor responses, linear, quadratic, and cubic spline interpolation are evaluated here. While both PCHIP and cubic spline interpolation use cubic polynomials for interpolation, the key difference lies therein that PCHIP is preserving monotonicity. PCHIP can therefore be understood as a conservative choice for interpolation of spectral sensor data, since no new maxima or minima are created during the interpolation process besides the sensor data points. In view of the curves (number of minima/maxima/saddle points) in the difference spectra to be estimated (Figure 6 - 8), it is clear why the simple 1st and 3rd order polynomials cannot keep up with the other methods, which perform very close to each other; depending on the metric considered,

TABLE 4. Result variations caused by using different interpolation algorithms in reconstructing the LEDs under stress after 2000 h operation with the minimal knowledge approach (without knowing the exact spectral sensitivities). Given are the mean and maximum resulting error metrics to compare the performance of the used interpolation method (polynomial and spline interpolations of varying order, piecewise cubic hermite interpolating polynomial).

Interpolation method	$\overline{\lvert\Delta E_\mathrm{r}\rvert}$/%	$\widehat{\lvert\Delta E_\mathrm{r}\rvert}$/%	$\overline{\lvert\Delta E_\mathrm{v}\rvert}$/%	$\widehat{\lvert\Delta E_\mathrm{v}\rvert}$/%	$\overline{\Delta u'v'} \cdot 10^{-3}$	$\widehat{\Delta u'v'} \cdot 10^{-3}$	$\overline{\mathrm{nRMSE}}$	$\widehat{\mathrm{nRMSE}}$
PCHIP	0.5134	1.2691	0.4494	0.6615	0.0022	0.0060	0.0114	0.0306
Poly1	0.6292	1.6218	0.9572	1.9073	0.0047	0.0097	0.0212	0.0451
Poly3	0.6814	1.7600	0.7867	1.5562	0.0041	0.0091	0.0185	0.0428
Poly7	0.4868	1.2460	0.3677	0.4842	0.0021	0.0059	0.0112	0.0319
Poly11	0.3004	0.5417	0.4306	0.6100	0.0021	0.0060	0.0126	0.0336
piecewise linear	0.5000	1.2715	0.4534	0.6535	0.0022	0.0061	0.0114	0.0312
piecewise quadratic	0.5193	1.2852	0.4341	0.6001	0.0021	0.0059	0.0110	0.0302
piecewise cubic	0.5235	1.2937	0.4362	0.6039	0.0021	0.0059	0.0110	0.0301

the ranking of the interpolation methods changes only slightly. The higher order polynomials provide slightly better radiometric or photometric results, although this is at the expense of colorimetric and spectral accuracy. The piecewise interpolation methods provide practically equivalent results. Therefore, the preservation of monotonicity by the PCHIP method does not provide clear advantages for the monitoring of the tested LEDs, degradation processes and the sensor used, but it is also not inferior to other methods.

From the data of the experiment presented here, a conclusion can be drawn to the question which method is best suited for monitoring LEDs with different aging properties: For LEDs that only loose flux without major spectral shifts, the PCHIP approach is predestined, as it does not require any complex sensor calibration and still shows excellent reconstruction results for these LEDs. For LEDs that are expected to have spectral shifts at wavelengths where there are also high radiation components in the initial spectrum, the Wiener filter adapted to the initial state provides the best reconstruction results. As long as these spectral shifts are wide enough, i.e., in the order of magnitude of the sensor channel width, the reconstruction results of the PCHIP approach are still suitable for application. For LEDs whose age-related spectral changes do not occur where there is a lot of radiant power in the initial spectrum or where anomalies, such as phosphor cracks, are observed, the conclusion is more difficult. Although the use of a spectral sensor provides an estimate of the actual LED emission that provides at least a halving of the color and a reduction of the relative radiometric error by at least 87 % compared to neglecting the degradation, the limit of this methodology for the reconstruction of color and spectral information from sensor data is reached.

The projection from SPD to sensor response that occurs inside a spectral sensor is a drastic reduction in dimension and information (401 wavelengths to a few sensor channels). Each sensor channel has a spectral width of its sensitivity, so the output of a sensor channel not only corresponds to the SPD at the peak wavelength, but it is a weighted (with the channel sensitivity) integral of the SPD. This introduces the problem of sensor metamerism: Different SPDs can cause the same sensor response, and therefore the inverse projection (sensor response to SPD) is not unique. Given a sensor response, accurate reconstruction of the original SPD (interpretation of the sensor response) therefore requires additional (a priori) information about the SPD, even if the sensor channel sensitivities are known. The task of extracting this a priori information and incorporating it into the reconstruction, but keeping the degree of estimation freedom large enough to have generalization and not create an overfit to the observed data (data used for modeling / information extraction) is not trivial. The only solution to make interpretation / reconstruction from sensor data less challenging is to reduce the dimensionality mismatch of the inversion task. There are two evident possibilities: Increasing the spectral resolution of the sensor (more channels, reduced width of channels) or reducing the dimensionality of the SPD (possibly through parametric modeling of LED spectra) without loss of information. However, this would require SPD models capable of describing individual spectral LED degradation with a few unambiguous parameters and without noticeable errors. Unfortunately, such models do not exist today.

One constraint in the application of the spectral sensor used in this work is that the resolving power is closely related to the integration time. For very small emission changes of a very low-light LED, very long integration times are needed to achieve a usable signal-to-noise ratio. During this time, the luminaire emission and, if applicable, the ambient lighting must not change. Another limitation becomes relevant when several LED channels in a luminaire are to be monitored. The approaches presented in this paper assume that the sensor responses to each LED are acquired individually. In an application with multiple LED channels, sequential acquisition of the individual channels would therefore be necessary. Alternatively, each LED channel could be captured via its own sensor or hardware-based solutions could be developed that ensure that iteratively only the light of a specific LED channel falls onto the sensor. A software solution is also conceivable that can determine the proportions of the individual LED channels from a detected light mixture, e.g., over several measurements with slight variations.

Ambient light, which may enter the luminaire from outside falling onto the sensor, poses no hard limitation as long as

the signal to be measured is not completely overpowered by the ambient light. Either the ambient and luminaire measurements can be directly offset against each other (e.g., ambient measurement with the luminaire switched off, subtracting from the sum measurement) or spectral unmixing algorithms could be developed to determine the ambient light contributions to the sensor response for subtraction before the estimation of the LED SPD.

VI. CONCLUSION

One key area of LED research is modeling the lifetime under different operating conditions. While standardized approaches exist for estimating the radiant flux as a function of time, temperature, and current, the modeling of spectral emission as a function of these influencing variables is complex and, according to the current state of research, subject to large errors compared to real degradation. It is therefore currently not practicable to use modeled spectral degradation for aging compensation in multi-channel LED systems. Such compensations, however, could achieve significantly improved color and radiant flux consistency increasing the lifetime of the fixture for factory-calibrated light settings (e.g., pre-calculated channel mixtures for various correlated color temperatures). This work, in contrast to a priori modeling, thus investigated a different approach: The estimation of the actual spectral power distribution of a degrading LED from spectral sensor responses.

Four different LEDs were subjected to accelerated aging operating conditions and the spectral emission was measured with a spectroradiometer and simultaneously captured with a spectral sensor. The comparison of degradation spectra and sensor responses showed that most of the spectral degradation is actually captured in the sensor data, even though the spectral resolution of the sensor is much lower than that of the spectroradiometer. Over the four LEDs (green, warm white, and two neutral white) under stress conditions (2000 h, 1.1 A, 75°) the maximum radiometric error of neglecting the appearing degradation would have been 7.2 % and 20.5 % at the end of the experiment, respectively. The mean and maximum colorimetric (spectral) error from that same comparison were 0.00284 (0.0126) and 0.01080 (0.0484) in terms of $\Delta u'v'$ (nRMSE). Two methods for reconstruction of the actual LED spectra from the sensor responses were presented and tested on the collected data. While the adjusted Wiener filter approach, which makes use of spectral characterization of the sensor sensitivities, was able to basically reconstruct the degraded SPDs with a smaller colorimetric error, the PCHIP approach, only making use of datasheet information about peak sensitivity wavelengths of the sensor channels, resulted in only minimally larger colorimetric estimation errors but also excellent radiometric estimates. Even without spectral characterization of the sensor the PCHIP approach could thus provide estimates of the same SPDs with a maximum radiometric error (compared to a spectroradiometer measurement) of 1.4 %, maximum colorimetric error of 0.0062 $\Delta u'v'$, and maximum nRMSE of 0.0310. Knowledge of specific sensor sensitivities used in an adjusted Wiener filter for reconstruction resulted in a maximum radiometric error of 2.0 %, maximum colorimetric error of 0.00486 $\Delta u'v'$, and maximum nRMSE of 0.0177.

In all cases, the estimation errors were smaller than neglecting the degradation. These results demonstrate that a spectral sensor is capable of providing spectral estimates after heavy degradation with very little errors compared to measurements of a spectroradiometer. The highest errors here are caused by a single LED developing a phosphor crack which influenced the spatial radiation characteristics as well as the spectral emission. While being easily identifiable from the sensor responses (e.g. for a damage warning to the user) such an unforeseeable event limits the ability to estimate the actual SPD from the sensor responses without the a priori knowledge of the causing spectral changes. If this event, which is certainly unlikely in practical applications with safely designed operating parameters, is not taken into account, the adjusted Wiener filter (the PCHIP approach) achieves a maximum radiometric error of 0.6 % (0.73 %), a maximum colorimetric error of 0.001 (0.0017) $\Delta u'v'$, and a maximum spectral nRMSE error of 0.0071 (0.0097) compared to the spectroradiometric ground truth monitoring of the LED degradation. In summary, it can be stated that by using a spectral sensor, even without a detailed characterization of the sensor itself, the actual condition of LEDs can be monitored more accurately than what human perception would be able to differentiate.

Subsequent work should investigate more closely how well spectrally narrow changes can in particular be estimated via a sensor, for example using different (beyond green) monochromatic, non-phosphor-converted LEDs. In addition, the question must be answered how a spectral sensor should be used in practical applications to best record the emission that actually leaves the luminaire, especially when it comes to devices that do not have a mixing chamber but create a highly directional emission. In this context, the findings from the bursting of the phosphor in LED NW2 and the associated change in the spatial radiation characteristics must be taken into account. At the same time, when developing a commercial luminaire, the operating conditions would be specified in such a way that such drastic damage should not be possible. However, an integrated spectral sensor provides important information in any case that the spectral emission has changed drastically. Depending on the application, this is useful even if no perfect reconstruction of the degraded spectral emission (and thus only limited compensation by other LED channels in a multi-channel system) is possible, e.g. for automated maintenance warnings or anomaly detection.

It is also interesting to consider the use case of having a sensor in the luminaire while carrying out long-term tests in the factory. This approach would allow manufacturers to develop specific solutions (such as Wiener filters) that could be programmed as firmware updates in case of unexpected degradation. These custom solutions could be

used to remotely calibrate luminaires that exhibit similar behavior in terms of the temporal response of the sensors in the field, thereby resolving any issues that may arise.

While no sensor drift was observed in this experiment, which clearly demonstrated the feasibility and potential of spectral sensor feedback to track spectral emission during the degradation of an LED, dedicated tests should explicitly focus on the optical stability of the sensors. Ideally, these new aging tests should be carried out on complete light engines with an integrated sensor, in order to be able to take into account all possible interactions (e.g. chemical reactions, humidity, temperature, spatial dislocations, etc.) of the components under the stress conditions.

Compared to competing technologies for compensation of aging phenomena of LEDs, spectral sensors offer big advantages. The so-called constant light output (CLO), which some electronic ballasts offer as an option, does not take into account the actual LED condition (LED emission) but uses a pre-programmed curve to compensate for the expected decrease in luminous flux depending on the LED operating time. Because field data is generally not available and laboratory degradation data (most notably LM-80 reports, where measurements are made with LEDs operating continuously in a controlled and stable temperature environment [70]) is in contrast to typical real-world usage patterns that include degradation accelerated by thermal cycling [71], any predictions based on LM-80 (laboratory) data may differ from real-world performance [70]. This translates to the possibility of open-loop compensation (CLO) models greatly over- or under-compensating the actual LED degradation. Integrated spectral sensors could not only collect these field data for modelling, but could also be used directly for requirement-oriented re-adjustment (closed loop compensation).

A single photodiode (e.g. luminance sensor) can only detect an integral quantity and cannot deal with spectral shifts, i.e., as soon as the sensor is not perfectly matched in terms of sensitivity (radiometric or photometric), spectral shifts also cause radiometric or photometric errors. This problem does not affect a spectral sensor, because due to the multiple spectral channels an estimation of the integral quantity can be achieved with small errors (below 2 % even for extreme degradation events such as phosphor cracks).

Finally, the initially formulated goal should of course be pursued further in subsequent work: The compensation of spectral and colorimetric errors in mixtures of several LED channels, when the SPDs of the individual channels in the current operating state are estimated by spectral sensor feedback. Such a self-monitoring (and possibly self-calibrating) multi-LED channel light engine could be of great use in all applications where constant radiometric output and color (spectral) quality is required, for example in museums, film sets, sample lighting, and automated color inspection. In museums, accurate color representation of artifacts and exhibits is critical. On film sets, maintaining consistent lighting during shooting is essential for seamless color correction and visual effects in post-production. Automated color inspection systems would greatly benefit from such a self-monitoring and self-calibrating light engine. These systems require precise and consistent illumination to ensure accurate and reliable color measurements in industries such as printing, textiles, and product quality control. In conclusion, the further pursuit of LED monitoring using multi-channel spectral sensors could significantly advance lighting technology, offering innovative solutions for applications requiring consistent radiometric output and impeccable color quality.

REFERENCES

[1] W. D. van Driel, M. Schuld, B. Jacobs, F. Commissaris, J. van der Eyden, and B. Hamon, "Lumen maintenance predictions for LED packages," *Microelectron. Rel.*, vol. 62, pp. 39–44, Jul. 2016.

[2] G. Bobashev, N. G. Baldasaro, K. C. Mills, and J. L. Davis, "An efficiency-decay model for lumen maintenance," *IEEE Trans. Device Mater. Rel.*, vol. 16, no. 3, pp. 277–281, Sep. 2016.

[3] M. Buffolo, A. Caria, F. Piva, N. Roccato, C. Casu, C. De Santi, N. Trivellin, G. Meneghesso, E. Zanoni, and M. Meneghini, "Defects and reliability of GaN-based LEDs: Review and perspectives," *Phys. Status Solidi A*, vol. 219, no. 8, Apr. 2022, Art. no. 2100727.

[4] M. S. Ibrahim, J. Fan, W. K. C. Yung, Z. Wu, and B. Sun, "Lumen degradation lifetime prediction for high-power white LEDs based on the gamma process model," *IEEE Photon. J.*, vol. 11, no. 6, pp. 1–16, Dec. 2019.

[5] Illuminating Engineering Society, *Technical Memorandum: Projecting Long-Term Luminous, Photon, and Radiant Flux Maintenance of LED Light Sources. ANSI/IES TM-21-21*. New York, NY, USA: IES, 2021.

[6] F. Reifegerste and J. Lienig, "Modelling of the temperature and current dependence of LED spectra," *J. Light Vis. Environ.*, vol. 32, no. 3, pp. 288–294, 2008.

[7] A. Vaskuri, P. Kärhä, H. Baumgartner, O. Kantamaa, T. Pulli, T. Poikonen, and E. Ikonen, "Relationships between junction temperature, electroluminescence spectrum and ageing of light-emitting diodes," *Metrologia*, vol. 55, no. 2, pp. S86–S95, Apr. 2018.

[8] A. Vaskuri, H. Baumgartner, P. Kärhä, G. Andor, and E. Ikonen, "Modeling the spectral shape of InGaAlP-based red light-emitting diodes," *J. Appl. Phys.*, vol. 118, no. 20, Nov. 2015, Art. no. 203103.

[9] B.-M. Song and B. Han, "Spectral power distribution deconvolution scheme for phosphor-converted white light-emitting diode using multiple Gaussian functions," *Appl. Opt.*, vol. 52, no. 5, p. 1016, 2013.

[10] Z. Guo, T. Shih, Y. Gao, Y. Lu, L. Zhu, G. Chen, Y. Lin, J. Zhang, and Z. Chen, "Optimization studies of two-phosphor-coated white light-emitting diodes," *IEEE Photon. J.*, vol. 5, no. 2, pp. 8200112–8200112, Apr. 2013.

[11] A. Keppens, W. R. Ryckaert, G. Deconinck, and P. Hanselaer, "Modeling high power light-emitting diode spectra and their variation with junction temperature," *J. Appl. Phys.*, vol. 108, no. 4, Aug. 2010, Art. no. 043104.

[12] M. E. Raypah, M. Devarajan, and F. Sulaiman, "Modeling spectra of low-power SMD LEDs as a function of ambient temperature," *IEEE Trans. Electron Devices*, vol. 64, no. 3, pp. 1180–1186, Mar. 2017.

[13] W. Chen, J. Fan, C. Qian, B. Pu, X. Fan, and G. Zhang, "Reliability assessment of light-emitting diode packages with both luminous flux response surface model and spectral power distribution method," *IEEE Access*, vol. 7, pp. 68495–68502, 2019.

[14] H. Chen and S. Y. Hui, "Dynamic prediction of correlated color temperature and color rendering index of phosphor-coated white light-emitting diodes," *IEEE Trans. Ind. Electron.*, vol. 61, no. 2, pp. 784–797, Feb. 2014.

[15] J. Fan, M. G. Mohamed, C. Qian, X. Fan, G. Zhang, and M. Pecht, "Color shift failure prediction for phosphor-converted white LEDs by modeling features of spectral power distribution with a nonlinear filter approach," *Materials*, vol. 10, no. 7, p. 819, Jul. 2017.

[16] J. Fan, Y. Li, I. Fryc, C. Qian, X. Fan, and G. Zhang, "Machine-learning assisted prediction of spectral power distribution for full-spectrum white light-emitting diode," *IEEE Photon. J.*, vol. 12, no. 1, pp. 1–18, Feb. 2020.

[17] J. Fan, W. Chen, W. Yuan, X. Fan, and G. Zhang, "Dynamic prediction of optical and chromatic performances for a light-emitting diode array based on a thermal-electrical-spectral model," *Opt. Exp.*, vol. 28, no. 9, p. 13921, 2020.
[18] C. Qian, J. Fan, X. Fan, and G. Zhang, "Prediction of lumen depreciation and color shift for phosphor-converted white light-emitting diodes based on a spectral power distribution analysis method," *IEEE Access*, vol. 5, pp. 24054–24061, 2017.
[19] S. Benkner, A. Herzog, S. Klir, W. D. Van Driel, and T. Q. Khanh, "Advancements in spectral power distribution modeling of light-emitting diodes," *IEEE Access*, vol. 10, pp. 83612–83619, 2022.
[20] J. Hegedüs, G. Hantos, and A. Poppe, "Lifetime modelling issues of power light emitting diodes," *Energies*, vol. 13, no. 13, p. 3370, Jul. 2020.
[21] Z. Vaitonis, A. Miasojedovas, A. Novičkovas, S. Sakalauskas, and A. Žukauskas, "Effect of long-term aging on series resistance and junction conductivity of high-power InGaN light-emitting diodes," *Lithuanian J. Phys.*, vol. 49, no. 1, pp. 69–74, 2009.
[22] A. Herzog, M. Wagner, and T. Q. Khanh, "Monitoring the optical degradation of green light-emitting diodes on the basis of measured electrical characteristics," *Microelectron. Rel.*, vol. 121, Jun. 2021, Art. no. 114147.
[23] A. Alexeev, J.-P. Linnartz, G. Onushkin, K. Arulandu, and G. Martin, "Dynamic response-based LEDs health and temperature monitoring," *Measurement*, vol. 156, May 2020, Art. no. 107599.
[24] W. D. van Driel and X. J. Fan, *Solid State Lighting Reliability: Components to Systems* (Solid State Lighting Technology and Application Series). New York, NY, USA: Springer, 2013.
[25] M. Buffolo, C. De Santi, M. Meneghini, D. Rigon, G. Meneghesso, and E. Zanoni, "Long-term degradation mechanisms of mid-power LEDs for lighting applications," *Microelectron. Rel.*, vol. 55, nos. 9–10, pp. 1754–1758, Aug. 2015.
[26] V. Q. Trinh, S. Babilon, P. Myland, and T. Q. Khanh, "Processing RGB color sensors for measuring the circadian stimulus of artificial and daylight light sources," *Appl. Sci.*, vol. 12, no. 3, p. 1132, Jan. 2022.
[27] J. Agudo, P. Pardo, H. Sánchez, Á. Pérez, and M. Suero, "A low-cost real color picker based on Arduino," *Sensors*, vol. 14, no. 7, pp. 11943–11956, Jul. 2014.
[28] J. Botero-Valencia, F. López-Giraldo, and J. Vargas-Bonilla, "Calibration method for correlated color temperature (CCT) measurement using RGB color sensors," in *Proc. Symp. Signals, Images Artif. Vis. (STSIVA)*, Bogota, Colombia, Sep. 2013, pp. 3–8.
[29] C. S. McCamy, "Correlated color temperature as an explicit function of chromaticity coordinates," *Color Res. Appl.*, vol. 17, no. 2, pp. 142–144, Apr. 1992.
[30] J.-S. Botero, F.-E. López, and J.-F. Vargas, "Classification of artificial light sources and estimation of color rendering index using RGB sensors, K nearest neighbor and radial basis function," *Int. J. Smart Sens. Intell. Syst.*, vol. 8, no. 3, pp. 1505–1524, Jan. 2015.
[31] L. Breniuc, C.-G. Haba, C.-D. Galatanu, D. Petrisor, and R. Hertanu, "Correlated color temperature measuring and adjustment system," in *Proc. 11th Int. Symp. Adv. Topics Electr. Eng. (ATEE)*, Piscataway, NJ, USA, Mar. 2019, pp. 1–6.
[32] I. Chew, V. Kalavally, C. P. Tan, and J. Parkkinen, "A spectrally tunable smart LED lighting system with closed-loop control," *IEEE Sensors J.*, vol. 16, no. 11, pp. 4452–4459, Jun. 2016.
[33] P. Maiti and B. Roy, "Evaluation of a daylight-responsive, iterative, closed-loop light control scheme," *Lighting Res. Technol.*, vol. 52, no. 2, pp. 257–273, Apr. 2020.
[34] M. Ashibe, M. Miki, and T. Hiroyasu, "Distributed optimization algorithm for lighting color control using chroma sensors," in *Proc. IEEE Int. Conf. Syst., Man Cybern.*, Los Alamitos, CA, USA: IEEE Computer Society, Oct. 2008, pp. 174–178.
[35] J.-S. Botero-Valencia, J. Valencia-Aguirre, D. Durmus, and W. Davis, "Multi-channel low-cost light spectrum measurement using a multilayer perceptron," *Energy Buildings*, vol. 199, pp. 579–587, Sep. 2019.
[36] A. Amirazar, M. Azarbayjani, M. Molavi, and M. Karami, "A low-cost and portable device for measuring spectrum of light source as a stimulus for the human's circadian system," *Energy Buildings*, vol. 252, Dec. 2021, Art. no. 111386.
[37] J.-S. Botero, J. V. Aguirre, and J.-F. V. Bonilla, "Estimation of light source color rendition with low-cost sensors using multilayer perceptron and extreme learning machine," *LEUKOS*, vol. 17, no. 3, pp. 280–290, Jul. 2021.
[38] A. Herzog, M. Wagner, and T. Q. Khanh, "Efficiency droop in green InGaN/GaN light emitting diodes: Degradation mechanisms and initial characteristics," *Microelectron. Rel.*, vol. 112, Sep. 2020, Art. no. 113792.
[39] A. Herzog, S. Benkner, B. Zandi, M. Buffolo, W. D. Van Driel, M. Meneghini, and T. Q. Khanh, "Lifetime prediction of current- and temperature-induced degradation in silicone-encapsulated 365 nm high-power light-emitting diodes," *IEEE Access*, vol. 11, pp. 19928–19940, 2023.
[40] P. L. Vora, J. E. Farrell, J. D. Tietz, and D. H. Brainard, *Digital Color Cameras-1-Response Models*. Palo Alto, CA, USA: Hewlett-Packard Laboratories, 1997.
[41] P. Myland, S. Babilon, and T. Q. Khanh, "Tackling heterogeneous color registration: Binning color sensors," *Sensors*, vol. 21, no. 9, p. 2950, Apr. 2021.
[42] P. Myland, S. Babilon, T. Hegemann, S. Klir, and T. Q. Khanh, "Reconstruction of spectral irradiance in a real application with a multi-channel spectral sensor using convolutional neural networks," *Opt. Exp.*, vol. 31, no. 16, p. 25724, Jul. 2023.
[43] W. Pratt, *Digital Image Processing: PIKS Inside*. Hoboken, NJ, USA: Wiley, 2001.
[44] N. Shimano, "Recovery of spectral reflectances of objects being imaged without prior knowledge," *IEEE Trans. Image Process.*, vol. 15, no. 7, pp. 1848–1856, Jul. 2006.
[45] P. Stigell, K. Miyata, and M. Hauta-Kasari, "Wiener estimation method in estimating of spectral reflectance from RGB images," *Pattern Recognit. Image Anal.*, vol. 17, no. 2, pp. 233–242, Jun. 2007.
[46] P. Urban, M. R. Rosen, and R. S. Berns, "A spatially adaptive Wiener filter for reflectance estimation," in *Proc. Color Imag. Conf.*, 2008, vol. 16, no. 1, pp. 279–284.
[47] P. Urban, M. R. Rosen, and R. S. Berns, "Spectral image reconstruction using an edge preserving spatio-spectral Wiener estimation," *J. Opt. Soc. Amer. A, Opt. Image Sci.*, vol. 26, no. 8, p. 1868, 2009.
[48] I. Nishidate, T. Maeda, K. Niizeki, and Y. Aizu, "Estimation of melanin and hemoglobin using spectral reflectance images reconstructed from a digital RGB image by the Wiener estimation method," *Sensors*, vol. 13, no. 6, pp. 7902–7915, Jun. 2013.
[49] S. Babilon, P. Myland, J. Klabes, J. Simon, and T. Q. Khanh, "Spectral reflectance estimation of organic tissue for improved color correction of video-assisted surgery," *J. Electron. Imag.*, vol. 27, no. 5, p. 1, Sep. 2018.
[50] A. Mahmoudi Nahavandi, "Noise segmentation for improving performance of Wiener filter method in spectral reflectance estimation," *Color Res. Appl.*, vol. 43, no. 3, pp. 341–348, Jun. 2018.
[51] F. Sippel, J. Seiler, N. Genser, and A. Kaup, "Structure-preserving spectral reflectance estimation using guided filtering," *J. Opt. Soc. Amer. A, Opt. Image Sci.*, vol. 37, no. 11, p. 1695, 2020.
[52] V. Kitanovski, J.-B. Thomas, and J. Y. Hardeberg, "Reflectance estimation from snapshot multispectral images captured under unknown illumination," *Color Imag. Conf.*, vol. 29, no. 1, pp. 264–269, Nov. 2021.
[53] J. Klein, J. Brauers, and T. Aach, "Methods for spectral characterization of multispectral cameras," in *Proc. SPIE*, F. H. Imai and F. Xiao, Eds. 2011, p. 78760B.
[54] Y. Murakami, K. Fukura, M. Yamaguchi, and N. Ohyama, "Color reproduction from low-SNR multispectral images using spatio-spectral Wiener estimation," *Opt. Exp.*, vol. 16, no. 6, p. 4106, 2008.
[55] H. Haneishi, T. Hasegawa, A. Hosoi, Y. Yokoyama, N. Tsumura, and Y. Miyake, "System design for accurately estimating the spectral reflectance of art paintings," *Appl. Opt.*, vol. 39, no. 35, p. 6621, 2000.
[56] H.-L. Shen and J. H. Xin, "Spectral characterization of a color scanner by adaptive estimation," *J. Opt. Soc. Amer. A, Opt. Image Sci.*, vol. 21, no. 7, p. 1125, 2004.
[57] H.-L. Shen, J. H. Xin, and S.-J. Shao, "Improved reflectance reconstruction for multispectral imaging by combining different techniques," *Opt. Exp.*, vol. 15, no. 9, p. 5531, 2007.
[58] S. Chen and Q. Liu, "Modified Wiener estimation of diffuse reflectance spectra from RGB values by the synthesis of new colors for tissue measurements," *J. Biomed. Opt.*, vol. 17, no. 3, 2012, Art. no. 030501.
[59] J.-H. Yoo, W.-J. Kyung, H.-G. Ha, and Y.-H. Ha, "Estimation of reflectance based on properties of selective spectrum with adaptive Wiener estimation," in *Proc. SPIE*, R. Eschbach, G. G. Marcu, and A. Rizzi, Eds. 2013, Art. no. 86520D.
[60] S. Tominaga and H. Sakai, "Spectral reflectance estimation from camera responses using local optimal dataset," *J. Imag.*, vol. 9, no. 2, p. 47, Feb. 2023.

[61] W. K. Pratt, "Generalized Wiener filtering computation techniques," *IEEE Trans. Comput.*, vol. COM-21, no. 7, pp. 636–641, Jul. 1972.
[62] U. Spagnolini, *Statistical Signal Processing in Engineering*. Hoboken, NJ, USA: Wiley, 2018.
[63] CIE, "Recommended practice for tabulating spectral data for use in colour computations," Int. Commission Illumination, Vienna, Austria, Tech. Rep. CIE 167:2005, 2005.
[64] K. A. Novak, *Numerical Methods for Scientific Computing: The Definitive Manual for Math Geeks*, 2nd ed. Arlington, VA, USA: Equal Share Press, 2022.
[65] S. Benkner, S. Babilon, A. Herzog, and T. Q. Khanh, "Combined methodology for accurate evaluation of distance and direction of chromaticity shifts in LED reliability tests," *IEEE Trans. Device Mater. Rel.*, vol. 21, no. 4, pp. 500–507, Dec. 2021.
[66] P. L. Vora, J. E. Farrell, J. D. Tietz, and D. H. Brainard, *Digital Color Cameras–2–Spectral Response*. Hewlett-Packard Laboratories, 1997.
[67] B. Jähne, "EMVA 1288 standard for machine vision," *Optik Photonik*, vol. 5, no. 1, pp. 53–54, Apr. 2010.
[68] G. Finlayson, M. M. Darrodi, and M. Mackiewicz, "Rank-based camera spectral sensitivity estimation," *J. Opt. Soc. Amer. A, Opt. Image Sci.*, vol. 33, no. 4, p. 589, 2016.
[69] Y. Ji, Y. Kwak, S. M. Park, and Y. L. Kim, "Compressive recovery of smartphone RGB spectral sensitivity functions," *Opt. Exp.*, vol. 29, no. 8, p. 11947, 2021.
[70] L. Davis and M. Hansen. *Led Luminaire Reliability: Impact of Color Shift*. U.S. Dept. Energy. Accessed: Sep. 28, 2023. [Online]. Available: https://www.energy.gov/sites/prod/files/2019/10/f67/lsrc_colorshift_apr2017.pdf
[71] M. P. Royer. (Dec. 2014). *Lumen and Chromaticity Maintenance of Led Par38 Lamps Operated in Steady-State Conditions*. U.S. Dept. Energy. Accessed: Sep. 28, 2023. [Online]. Available: https://doi.org/10.2172/1170114

PAUL MYLAND received the M.S. degree in electrical engineering and information technology from the Technical University of Darmstadt, Germany, in 2019. He is currently pursuing the Ph.D. degree with the Laboratory of Adaptive Lighting Systems and Visual Processing. Since then, he has been with the Laboratory of Adaptive Lighting Systems and Visual Processing as a Research Assistant. His current work is focused on applications for spectral sensors in lighting control. His broader research interests include color and lighting quality, color perception, museum lighting, and multidimensional lighting optimization.

ALEXANDER HERZOG received the B.Sc., M.Sc., and Ph.D. degrees in electrical engineering from Technische Universität Darmstadt, in 2012, 2015, and 2020, respectively. He is currently a Postdoctoral Researcher and the Research Group Leader of the Laboratory of Adaptive Lighting Systems and Visual Processing, Technische Universität Darmstadt. His research interests include lifetime prediction, reliability analysis, digital twins of light-emitting diodes, temporal light artifacts, and spectral optimization of metameric spectra.

SEBASTIAN BABILON received the Ph.D. degree in electrical engineering from Technische Universität Darmstadt, in 2018. His work mainly focused on color perception and the modeling of color rendition in relation to memory colors. After three years of being appointed as a Postdoctoral Researcher, he moved on to industrial research and development. Currently, he is with Arnold & Richter Cine Technik GmbH & Co. Betriebs KG as a Development Engineer being responsible for the colorimetric design and optimization of lighting fixtures for the movie and television industry.

WILLEM D. VAN DRIEL received the Graduate degree in mechanical engineering from the Technical University of Eindhoven and the Ph.D. degree from Delft University of Technology, The Netherlands. He has more than 25 years of track record in the reliability domain. Application areas range from healthcare, gas and oil explorations, and semiconductors. He is currently a Fellow Scientist with Signify (formerly Philips Lighting). Besides that, he was a Professor with the University of Delft, The Netherlands. He has authored or coauthored more than 350 scientific publications, including journals and conference papers, book or book chapters, and invited keynote lectures. His research interests include solid state lighting, microelectronics and microsystems technologies, virtual prototyping, virtual reliability qualification, and designing for reliability of microelectronics and microsystems. He is the Chair of the Organizing Committee of the IEEE Conference EuroSimE.

TRAN QUOC KHANH received the Graduate degree in optical technologies and the Ph.D. degree in lighting engineering from the Technical University of Ilmenau, Germany. He is currently an University Professor and the Head of the Laboratory of Adaptive Lighting Systems and Visual Processing, Technical University of Darmstadt, Germany. Before being appointed as a Professor, he gathered industrial experience as a project manager with Arnold and Richter Cine Technik AG, Munich, Germany. His research interests include modern lighting technology, including LEDs, colorimetry, mesopic vision, glare, photometry, and color science related topics.